Journal of Volcanology and Geothermal Research 341 (2017) 242–254

Contents lists available at ScienceDirect

Journal of Volcanology and Geothermal Research

journal homepage: www.elsevier.com/locate/jvolgeores

Contrasting P-T paths of shield and rejuvenated volcanism at Robinson Crusoe Island, Juan Fernández Ridge, SE Pacific

Javier Reyes [a,b,*], Luis E. Lara [c], Diego Morata [a,b]

[a] Departamento de Geología, Facultad de Ciencias Físicas y Matemáticas, Universidad de Chile, Santiago, Chile
[b] Centro de Excelencia en Geotermia de Los Andes, Santiago, Chile
[c] Volcano Hazards Program, Servicio Nacional de Geología y Minería, Santiago, Chile

ARTICLE INFO

Article history:
Received 30 January 2017
Received in revised form 5 May 2017
Accepted 30 May 2017
Available online 9 June 2017

ABSTRACT

A remarkable expression of intraplate volcanism is the occurrence of evolutionary stages with important variations of magmatic processes and products. Plumbing systems and storage conditions seem to be different for shield and rejuvenated volcanism, two classical stages notably preserved in Robinson Crusoe Island, Juan Fernández Ridge in the SE Pacific Ocean. We here present first order geochemical features for rocks from both shield and rejuvenated stages and through geothermobarometry and textural analysis we unravel their contrasting ascent and storage history. The shield stage (~3.8 Ma) is represented by a ~900 m thick sequence of basalt, picrobasalt and picrite lava flows forming subsets according their chemistry and mineralogy: 'differentiated', 'near-primitive' and 'olivine-rich' lavas. Pressure estimates for in equilibrium assemblages are <3.2 kbar, and temperature ranges around 1321 °C for the 'near-primitive' and 1156–1181 °C for the 'differentiated' groups. Volcanic rocks from the rejuvenated stage (~0.9 Ma) fill the eroded morphology of the shield pile with basanite and picrite lava flows with two compositional varieties: the primitive 'high-Mg' group that crystallized clinopyroxene at pressures <3.7 kbar and olivine at temperatures in the range 1316–1354 °C; and the 'low-Mg' group that carries notably zoned crystals formed at a wide range of pressures (0–10.8 kbar) and temperatures (1256–1295 °C). This allows us to infer contrasting patterns of ascent and storage during these archetypical stages in Robinson Crusoe Island, which also controlled volcanic processes on surface and finally shaped the island. We propose the existence of shallow magmatic reservoirs in the shield stage, where the ascending magmas would have been stored and differentiated. On the other hand, rejuvenated magmas experimented rapid ascent with polybaric crystallization and sometimes short-time storage in low-volume reservoirs. Similar conditions have been proposed in other oceanic islands suggesting that shallow reservoirs in the shield stage and deeper crystallization of more alkaline magmas in the rejuvenated stage seems to describe a global pattern.

1. Introduction

Intraplate volcanoes are related to primary mantle plumes (e.g., Courtillot et al., 2003) and serve as virtual windows to the deep Earth's mantle. Pioneering work by Morgan (1971, 1972a, 1972b) introduced the hypothesis of fixed mantle plumes, hot and enriched, able to melt by decompression. One of the most evident results of such an origin is the observed age progression of volcanic rocks from oceanic islands and/or seamounts along a chain. However, a number of volcanic alignments do not satisfy this condition, as observed by Clouard and Bonneville (2001) for the Pacific Ocean basin. Alternative ideas have been proposed as non-fixed plumes (Steinberger and O'Connell, 1998) or tectonically-controlled decompression related to magmatic hydrofracture driven by flexural stresses in presence of a volcanic load (Hieronymus and Bercovici, 2000). More frequent processes as subduction cooling, continental insulation, small-scale convection in presence of ridges, rifts and fracture zones (Anderson, 2000, 2001) or small-scale sublithospheric convections (Ballmer et al., 2007) could also explain the array of hotspot volcanoes on oceanic plates.

'Wet' or volatile-rich plumes without high temperatures have also been proposed (Bonatti, 1990; Nichols et al., 2002), which fuels the controversy about the source and P-T conditions for intraplate volcanism.

The archetypical evolutionary model of oceanic islands (based on the Hawaiian case, e.g., Garcia et al., 2015) includes the pre-shield (alkaline submarine volcanism), shield (voluminous tholeiitic submarine and subaerial volcanism) and post-shield stages (alkaline pulses). The geochemical and isotopic differences for those three stages are usually explained by variations in the degree of partial melting and some changes in the mantle source composition (Frey et al., 1990).

* Corresponding autor at: Departamento de Geología, Facultad de Ciencias Físicas y Matemáticas, Universidad de Chile, Santiago, Chile.
E-mail addresses: jareyes@ing.uchile.cl (J. Reyes), luis.lara@sernageomin.cl (L.E. Lara), dmorata@cec.uchile.cl (D. Morata).

http://dx.doi.org/10.1016/j.jvolgeores.2017.05.035
0377-0273/

Sometimes, after a period of quiescence, a rejuvenated stage (Ozawa et al., 2005) is recognized, consisting in a small volume of alkaline magmatism. The origin of this late stage of volcanism is still controversial, despite the growing amount of occurrences, first recognized at Hawaii (Macdonald et al., 1983; Garcia et al., 2010) and then in Samoa (Wright and White, 1987; Konter and Jackson, 2012), Marquesas (Woodhead, 1992), Canary Islands (Hoernle and Schmincke, 1993), Society (White and Duncan, 1996), Kerguelen (Weis et al., 1998), Madeira (Geldmacher and Hoernle, 2000), Mauritius (Paul et al., 2005) and Fieberling-Guadalupe (Konter et al., 2009).

A number of models have been proposed for the origin of the rejuvenated stage: (1) thermal effect of a mantle plume that melts the surrounding oceanic lithosphere (e.g., Gurriet, 1987); (2) secondary melting zone in the plume as a result of internal convection and lateral spreading beneath the lithosphere (e.g., Ribe and Christensen, 1999); (3) decompression melting of the plume due to a flexure of the oceanic plate generated by the construction of new shield volcanoes on top (e.g., Bianco et al., 2005); and (4) small-scale sublithospheric convection in the ambient mantle and spreading plume (Ballmer et al., 2011). Each oceanic hotspot may (or may not) develop the volcanic stages described (pre-shield, shield, postshield and rejuvenated) displaying variations in the chemistry, petrography, and erupted volume.

The magmatic plumbing and storage for shield and post-shield stages have an extended effect on both eruptive style and morphological evolution of oceanic islands and seamounts. P-T paths retrieved from mineral chemistry can track the ascent and storage history. For example, shallow reservoirs have been inferred (and independently tested by geophysical tools) in Hawaii for the shield stage (Ryan, 1988; Poland et al., 2014; Tilling et al., 2014; Pietruszka et al., 2015), but a deeper storage region was inferred for the post-shield stage (Frey et al., 1990), either in the mantle (Chatterjee et al., 2005) or within the crust (Hammer et al., 2016).

Rejuvenated volcanism seems to be more complex in origin implying different sources and ascent pathways. Here we characterize first order geochemical features of both shield and rejuvenated stages in Robinson Crusoe Island. Through geothermobarometry and textural analysis we unravel their ascent and storage history.

2. Juan Fernández Ridge

An outstanding yet still poorly studied example of intraplate volcanism is the Juan Fernández Ridge, an aseismic ridge running for ca. 800 km over the Nazca Plate in the Southeast Pacific. The Juan Fernández Ridge obliquely converges (N80°E) with the South American margin at 33.4°S (Fig. 1) and is mostly built on top of a ca. 22–37 Ma old Nazca Plate (Rodrigo and Lara, 2014). Because of the isolation from active spreading ridges, it is a suitable target for understanding mantle signatures of the Southeast Pacific and general evolution of oceanic island/seamounts on a relatively fast moving plate (70.53 mm/yr eastward at present according to GEODVEL 2010 model; Argus et al., 2010).

Around 15 volcanoes comprise the Juan Fernández Ridge: Robinson Crusoe, Santa Clara, Alejandro Selkirk islands and at least 12 seamounts (>1000 m above the ocean floor, Fig. 1). The most important seamounts (from E to W) are O'Higgins, O'Higgins guyot (Vergara and Morales, 1985), Alpha (Farley et al., 1993) Beta, Gamma, Duke, Cinque Ports, Dresden (Rodrigo and Lara, 2014), Friday (Farley et al., 1993) and Domingo (Devey et al., 2000). Ar-Ar total fusion age for O′Higgins (~8.50 Ma; Von Huene et al., 1997) and K-Ar for Robinson Crusoe (~3.10–5.80 Ma) and Alejandro Selkirk (0.85–1.30 Ma; Booker et al.,

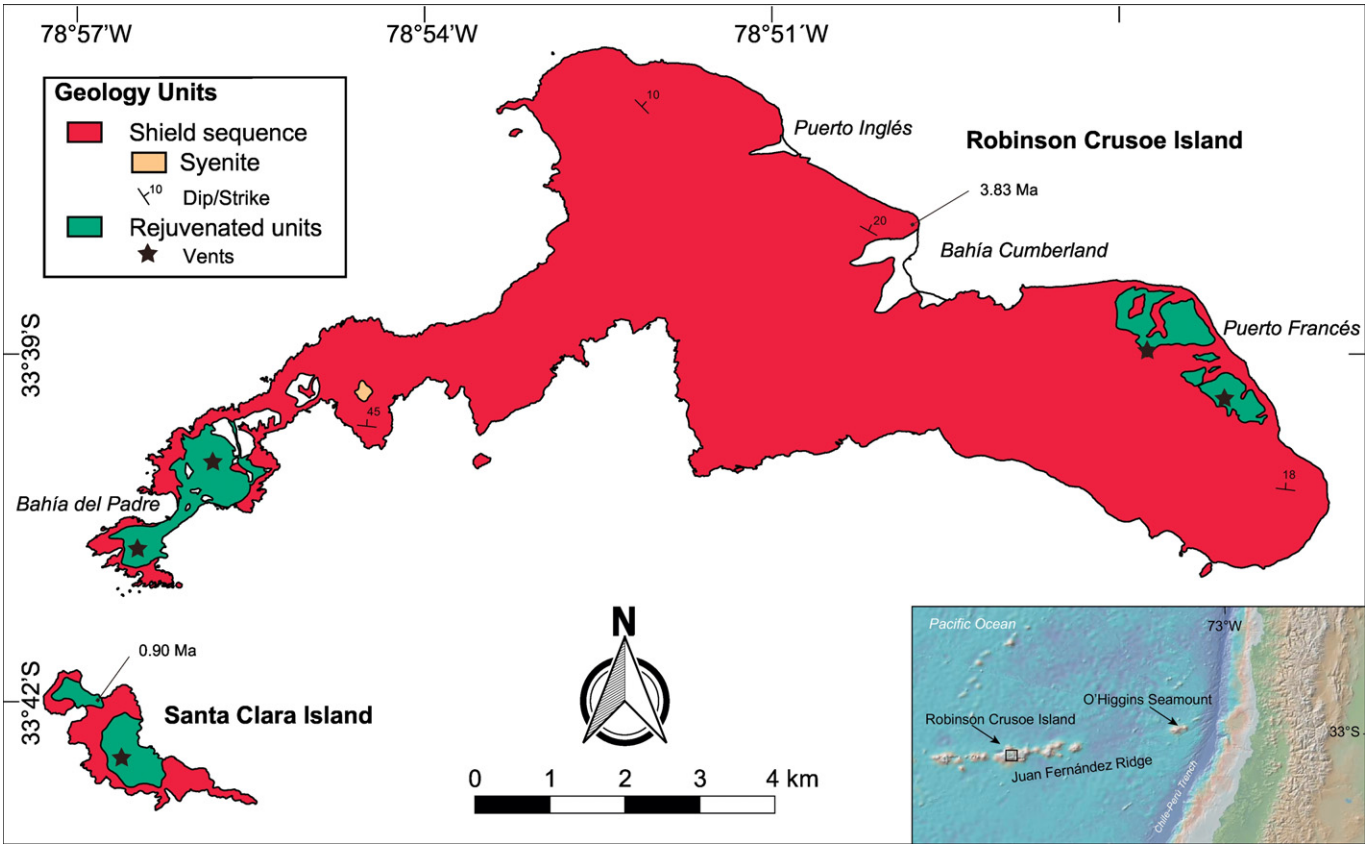

Fig. 1. Simplified geological map of Robinson Crusoe and Santa Clara Islands (modified from Morales, 1987) with main units as presented in the text. Dip/strike in shield sequence, vents of rejuvenated stage and $^{40}Ar/^{39}Ar$ age sites are showed. Inset shows the regional topography and bathymetry around the Juan Fernández Ridge.

1967; Stuessy et al., 1984) define a general age progression for shield stages and thus a fixed primary mantle plume would be implied.

Some geological studies were carried out in the past decades in Juan Fernández archipelago. The pioneer geological description of Robinson Crusoe and Alejandro Selkirk islands by Quensel (1920) (who reported some curiosities like the presence of trachytes and olivine-rich lavas called 'masafuerites' in reference to the former name 'Más Afuera' for Alejandro Selkirk Island) was followed by the geological reconnaissance of Robinson Crusoe Island by Morales (1987). A narrow field for $^{87}Sr/^{86}Sr$ and $^{143}Nd/^{144}Nd$ ratios was interpreted to indicate the involvement of a limited range of mantle components (Gerlach et al., 1986). Baker et al. (1987) and Farley et al. (1993) identified two different lithologies, basalts and basanites, as shield and post-shield units. The geochemical and isotopic ($^3He/^4He$ in olivine phenocrysts) differences were explained by transition from a typical plume for the first stage to a MORB-like source in the second one (Farley et al., 1993). Natland (2003) studied the morphology of olivine crystals and their capture of He concluding the existence of mixing between low and high temperature (olivine-charged) magmas. Furthermore, Devey et al. (2000) studied Friday and Domingo seamounts, which correspond to the westernmost volcanoes in Juan Fernández Ridge, reporting the presence of vesicular basalts, basanites and basaltic trachyandesites interpreted as products of metasomatic reactions between mantle harzburgites and a CO_2-bearing plume.

Geochronological data for Robinson Crusoe is scarce and based on imprecise K-Ar ages of 3.5 ± 0.8, 3.1 ± 0.9 (Booker et al., 1967) and 3.8 ± 0.2, 4.2 ± 0.2, 5.8 ± 2.1 (Stuessy et al., 1984). A sharp unconformity separates both the shield and rejuvenated units and is an evidence of erosion and volcanic quiescence in between.

3. Methods and analytical procedures

From the geological map and field reconnaissance, the main sequences or volcanic units were recognized and sampling sites chosen where sharp unconformity separates both the shield and post-shield units. Fresh whole-rocks were crushed to 250–180 μm grain sizes and handy-picked for extract major phenocrysts or weathered surfaces. Single aliquots were analyzed by incremental heating with a CO_2 laser at Servicio Nacional de Geología y Minería, Chile (SERNAGEOMIN). Clean samples were first placed in a disk of high purity aluminium together with a monitor grain of Fish Canyon sanidine (28.03 ± 0.1 Ma; Renne et al., 1994). Sealed disc was sent for irradiation to La Reina nuclear reactor (Chile), operated by the Comisión Chilena de Energía Nuclear. Both samples LL240711–1 and JR160913–2 were irradiated 21.95 h. Once the samples were received from the reactor, individual total fusion analyses were performed for all the monitors from the disk, and J factors are calculated for each grain, which represents an individual position in the disc. The distribution of J in 2 dimensions across the disc is modeled by a 2-dimensional quadratic fit to the data, resulting in a 'J surface' for the disc (e.g., Lara et al., 2006). Individual J factors for each sample are thus calculated depending upon the coordinates of the sample. The samples were analyzed by successive heating with increments of temperature by increases in the power of the laser using an integrative lens, which allows even heating of a plane of 6 × 6 mm (each sample hole has a diameter of 5 mm). The CO_2 laser has a maximum power of 30 W. Following each three heating steps a line blank was analyzed. Then, the noble gases were separated from the other evolved ones by means of a cold trap at ~133 °C and a ST101 getter operated at 2.2 A. Once purified the noble gases were introduced into a high resolution MAP 215–50 mass spectrometer in electron multiplier mode. The isotopes ^{36}Ar, ^{37}Ar, ^{38}Ar, ^{39}Ar and ^{40}Ar were analyzed in 10 cycles, and the $^{36}Ar/^{40}Ar$, $^{37}Ar/^{40}Ar$, $^{38}Ar/^{40}Ar$ and $^{39}Ar/^{40}Ar$ ratios were calculated for time zero to eliminate the effects of isotope fractionation during the analysis. The baseline was analyzed at the beginning and the end of the analysis, for each step, and subtracted from the peak heights. Spectrometer bias was corrected using periodic analyses of air samples, from which a correction factor (discrimination factor) was calculated. Two reproducible results were obtained from the step heating experiments. Each apparent age considers the corrections corresponding to isotopes of Ar associated with atmospheric argon, and argon that results from the irradiation of K, Ca and Cl. Plateaus were defined using the approach of Fleck et al. (1977). For a plateau to be valid, it must comprise three or more serial steps containing at least 50% of the total liberated ^{39}Ar, and the 2σ errors of these steps must overlap. When ^{40}Ar excess was detected, the isochrone age was preferred. When concordant plateau and isochrone ages were obtained, the plateau age was preferred because of its low uncertainty (Table S.1).

Petrographic analysis was made by optical microscopy and scanning electron microscopy (SEM FEI Quanta 250) at the Centro de Excelencia en Geotermia de Los Andes (CEGA) facilities of Universidad de Chile SERNAGEOMIN. Modal count (500 points) was performed in 20 samples (results in Table 1). Whole rock major element and Ni chemistry (55 samples) was analyzed at AcmeLabs, Vancouver, Canada. The rock chips crushed from field hand samples were fused with lithium metaborate/tetraborate and a dilute nitric acid digestion prior to major element analysis by ICP-ES. In addition a separate split was digested in Aqua Regia and analyzed by ICP-MS to report the Ni content. Loss on ignition (LOI) is by weigh difference after ignition at 1000 °C. Table 2 provides the analytical detection limits for each element used in this study. Precision and accuracy of the analyses were monitored by analysis of: recognized geochemical standards, split duplicate samples and AcmeLabs internal standards.

Olivine and clinopyroxene chemistry (20 samples) was measured by electronic microprobe (EPMA JEOL JXA 8230 equipped with three wavelength-dispersive spectrometers) at Laboratorio de Microscopía

Table 1
Petrography of Robinson Crusoe samples utilized in geothermobarometry estimations based on 500 point modes. Mineralogy reported as vesicle-free volume percent only for pheno and microphenocrysts (>0.2 mm in diameter). All samples used in clinopyroxene geobarometry. (O) used in olivine-liquid and (C) in clinopyroxene-liquid geothermometry. Rock type according mineralogy and chemistry. GM: groundmass. Ves: vesicles content.

		GM	Mineralogy				Ves
Sample	Rock type	(%)	Ol	Cpx	Plg	Op	(%)
Shield 'differentiated'							
LL230711–7(*)	Tholeiitic basalt	70	–	6	15	–	2
LL250711–1 (C)	Alkali basalt	64	5	10	21	–	4
LL260711–3	Tholeiitic basalt	80	6	4	10	–	13
JR160913–13 (C)	Tholeiitic basalt	99	–	1	–	–	1
LL220112–3 (O)(C)	Tholeiitic basalt	94	2	2	2	–	5
LL240711–1 (O)(C)	Alkali basalt	98	<1	<1	2	–	12
LL250711–9 (C)	Tholeiitic basalt	98	<1	1	1	–	4
Shield 'near-primitive'							
LL250711–7 (C)	Tholeiitic basalt	92	6	1	1	–	5
JR290513–2 (O)	Tholeiitic basalt	92	7	–	–	1	–
JR290513–5	Alkali basalt	93	2	3	2	–	3
Shield 'olivine-rich'							
LL250711–5	Tholeiitic basalt	75	25	–	–	–	–
Rejuvenated 'high-Mg'							
JR220112–3 (O)	Basanite	88	12	<1	–	–	3
JR250112–3 (O)	Picrite	87	12	1	–	–	2
Rejuvenated 'low-Mg'							
LL230711–2	Basanite	81	10	9	–	<1	<1
JR020613–3	Basanite	93	5	1	–	1	2
JR160913–2 (O)	Basanite	87	6	7	–	–	2
LL010213–6 (O)	Basanite	94	6	<1	–	<1	–
LL220112–4 (O)	Basanite	90	8	2	–	–	–
Xenoliths							
LL240711-5C	Dunite	–	96	–	2	2	
		Ol	Cpx	Opx	Spl	Gl	
JF-2A	Lherzolite	47	21	28	3	1	

Table 2
Major element (wt%) and Ni (ppm) concentrations of Robinson Crusoe Island lavas. $Fe_2O_3^T$: total iron as ferric. Loss-on-ignition (LOI) (wt%) is included.

Sample	SiO_2	TiO_2	Al_2O_3	$Fe_2O_3^T$	MgO	MnO	CaO	Na_2O	K_2O	P_2O_5	Ni	LOI	Sum
Det. limit	0.01	0.01	0.01	0.04	0.01	0.01	0.01	0.01	0.01	0.01	0.1	0.1	
Shield 'differentiated'													
LL230711–7	45.98	3.57	14.34	11.88	4.88	0.18	12.38	2.35	0.33	0.43	30.8	3.4	99.72
LL230112–1	46.03	3.28	14.97	11.31	6.77	0.15	9.49	2.90	1.05	0.48	67.9	3.1	99.53
JR300513–3	46.07	3.25	13.83	12.49	6.27	0.19	10.40	2.63	0.95	0.44	66.4	3.1	99.62
LL240711–1	47.03	3.61	14.56	12.67	5.77	0.17	10.24	2.98	1.00	0.50	31.7	1.1	99.63
LL240711–2	46.98	3.14	14.57	12.49	6.13	0.16	10.47	3.00	0.86	0.41	46.6	1.4	99.61
LL240711–6	46.58	3.58	15.38	12.24	5.40	0.15	10.01	3.06	0.91	0.51	39.9	1.8	99.62
LL260711–2	47.56	3.60	14.75	12.39	5.67	0.16	10.26	3.11	1.01	0.49	39.1	0.6	99.60
JR270513–1	45.18	3.77	16.01	13.69	5.55	0.16	8.10	2.72	0.85	0.56	79.5	3.0	99.59
LL250711–1	45.60	3.58	14.88	12.29	5.69	0.15	10.41	2.69	1.00	0.58	84.5	2.7	99.57
LL250711–3	45.97	3.76	15.33	12.95	5.13	0.15	8.99	3.19	1.17	0.63	105.2	2.3	99.57
LL220112–2	47.28	3.73	15.64	12.63	4.19	0.12	9.00	3.12	0.91	0.47	45.1	2.6	99.69
LL220112–3	47.53	3.35	14.21	12.58	6.75	0.16	10.40	2.79	0.88	0.43	80.7	0.6	99.68
LL220112–5	46.60	3.65	16.04	12.62	5.78	0.17	9.37	3.29	1.08	0.50	41.0	0.5	99.60
JR220112–2	46.94	3.36	14.26	12.53	5.63	0.16	10.11	3.12	1.03	0.47	35.8	2.1	99.71
JR250513–2	47.93	3.04	15.51	11.83	5.84	0.18	10.07	2.61	0.82	0.35	64.3	1.5	99.68
JR250513–4	48.59	3.23	15.28	11.50	6.15	0.16	10.51	2.92	0.93	0.41	49.9	0.0	99.68
JR250513–5	47.09	3.91	15.74	12.40	5.67	0.16	8.88	3.42	1.34	0.63	72.9	0.4	99.64
JR160913–1	46.44	3.38	14.79	12.50	5.39	0.12	9.59	2.49	0.66	0.41	84.6	3.4	99.17
JR160913–10	49.20	3.17	14.56	10.99	5.53	0.14	11.12	2.90	0.69	0.38	31.8	1.0	99.68
JR160913–13	47.87	3.51	14.69	11.39	5.18	0.14	11.08	3.04	0.90	0.42	35.8	1.4	99.62
LL250711–8	46.22	3.64	15.28	12.71	5.94	0.18	9.58	2.66	0.95	0.47	33.6	2.0	99.63
LL250711–9	47.18	3.42	14.78	12.48	6.24	0.17	10.56	2.76	0.80	0.39	34.8	0.9	99.68
LL250711–4	46.77	3.80	14.73	13.22	5.33	0.17	9.23	3.15	1.04	0.59	46.4	1.6	99.63
MP270112–4	45.41	3.79	15.32	13.65	6.70	0.16	9.02	2.86	1.10	0.54	110.6	1.1	99.65
Shield 'near-primitive'													
JR290513–5	45.42	3.31	13.43	12.06	9.11	0.17	9.28	2.68	1.31	0.42	265.5	2.4	99.59
JR290513–2	45.65	2.48	12.80	12.66	12.04	0.19	9.49	2.28	0.60	0.30	158.3	0.9	99.39
LL250711–7	45.89	2.96	13.38	12.48	8.42	0.15	9.70	2.60	0.64	0.34	193.9	3.0	99.56
LL300113–1	46.31	2.88	13.45	12.87	9.91	0.17	9.98	2.22	0.68	0.36	186.4	0.8	99.63
Shield 'olivine-rich'													
JR270513–2	45.07	3.05	10.98	14.36	14.82	0.18	7.14	2.52	0.93	0.41	558.4	−0.1	99.36
LL250711–5	45.46	1.83	10.37	13.66	17.47	0.17	7.20	2.02	0.34	0.20	583.4	0.6	99.32
JR250513–1	43.75	2.01	8.37	15.55	20.51	0.15	4.84	1.34	0.52	0.26	1098.6	1.8	99.10
LL040213–2	45.83	2.46	11.04	12.28	14.23	0.17	8.56	2.01	0.58	0.28	514.1	2.1	99.54
Rejuvenated 'high-Mg'													
JR250112–3	42.42	2.79	12.43	12.09	12.20	0.18	11.35	2.32	0.52	0.54	261.4	2.6	99.44
LL230112–2	41.32	2.73	12.58	12.75	13.31	0.19	10.31	2.43	1.33	0.58	273.1	1.7	99.23
LL230112–4	43.00	2.80	12.91	11.74	11.45	0.18	11.51	2.42	0.55	0.53	257.5	2.2	99.29
JR220112–3	42.62	2.75	12.66	12.40	13.09	0.19	10.92	3.40	0.70	0.48	250.9	0.2	99.41
Rejuvenated 'low-Mg'													
LL230711–2	42.15	2.80	13.77	12.30	10.22	0.21	10.58	2.83	0.59	0.62	182.1	3.3	99.37
LL230711–8	42.14	3.20	13.04	12.81	11.16	0.20	10.59	3.79	0.80	0.68	225.5	1.0	99.41
JR250112–2	42.02	3.08	13.06	13.15	10.81	0.20	10.08	3.45	0.56	0.64	233.7	2.4	99.45
LL060213–1	43.09	3.04	13.72	12.37	8.72	0.19	10.86	2.84	0.77	0.59	219.0	3.4	99.59
LL060213–3	41.69	3.18	13.95	13.17	8.86	0.21	10.50	2.39	1.18	0.89	148.9	3.4	99.42
LL060213–4	43.82	2.71	14.57	11.90	8.37	0.21	10.55	3.68	1.78	0.63	129.0	1.3	99.52
JR230112–1	42.19	3.18	13.10	13.10	11.04	0.20	10.78	3.88	0.78	0.61	172.5	0.6	99.46
JR230112–2	41.42	3.34	13.62	13.69	8.66	0.21	10.77	3.93	0.68	0.61	154.2	2.6	99.53
JR230112–3	42.99	2.91	13.43	13.77	9.52	0.23	9.81	3.79	1.70	0.91	142.4	0.4	99.46
JR160913–2	42.66	3.06	14.32	12.98	8.96	0.22	10.28	3.37	0.99	0.72	132.9	1.9	99.46
MP270112–3	44.59	2.63	13.42	12.51	9.94	0.23	9.28	3.74	1.71	0.74	224.4	0.6	99.39
JR020613–3	43.66	2.70	14.15	12.60	9.65	0.22	9.03	3.44	1.66	0.73	234.5	1.6	99.44
LL010213–6	43.81	3.18	14.10	13.87	8.54	0.22	9.51	3.53	1.83	0.78	135.2	0.2	99.57
JR220112–4A	44.06	3.07	14.17	12.92	8.43	0.21	10.03	4.16	0.92	0.65	141.7	0.9	99.52
LL220112–1	42.86	3.11	13.25	12.50	10.58	0.20	11.21	2.80	1.37	0.63	171.7	0.9	99.41
JR250513–3	41.99	3.07	13.91	13.27	10.22	0.21	10.57	1.76	0.75	0.68	207.1	3.0	99.43
LL220112–4	44.14	2.79	14.30	12.72	9.10	0.23	9.18	3.96	1.84	0.69	147.9	0.5	99.45
JR250513–9	43.69	2.85	13.98	13.57	9.72	0.23	8.00	2.82	1.87	0.95	245.4	1.7	99.38
LL020213–1	41.06	3.02	14.01	13.24	10.81	0.21	10.41	1.98	0.95	0.68	206.8	3.2	99.57

Electrónica y Análisis de Rayos X (LAMARX), Universidad Nacional de Córdoba, Argentina. Crystals used for the analysis were: TAP (Na, Mg, Al and Si), PET (Ca and Ti) and LiF (Cr, Mn, Fe and Ni) with an accelerating potential of 15.0 kV and electron beam current of 20 nA in 5 μm circles. Counting times were 10 s for peak and 5 s at each background position. Data reduction was performed using the ZAF correction method. Based on repeated analyses of standards, concentrations for major elements are accurate to within 1.5% (relative) for elements that exceed 10 wt%, about 5% for those between 10 and 1 wt%, and about 20% for those below 1 wt%. Precision is better than 0.6, 2 and 9% (relative), respectively. Tables S.3 and S.4 provides the analytical detection limits for each element used in this study. These are typical measurement conditions used in literature considered as 'routine analysis' and do not show high precision results (Sobolev et al., 2007) reflected in an error

of 0.26 in olivine forsterite content and 0.24 in clinopyroxene wollastonite content.

4. Results

4.1. Geological overview of shield and rejuvenated exposures

Shield stage in Robinson Crusoe Island forms a ca. 900 m thick sequence, with outstanding exposures in the sea cliffs. The island is built on a submarine pedestal (>2000 m high) probably formed by pre-shield and shield volcanic rocks. Baker et al. (1987) proposed a scheme with central and peripheral vents but early reconnaissance by Morales (1987) and our more detailed field mapping favor a central structure with a gently dipping shield sequence cross cut by dyke complexes (Fig. 2a), which in turn is covered with unconformity by the rejuvenated unit (Fig. 2b). The latter is defined by several small and isolated vents with related lavas and pyroclastic beds (Fig. 1). Feeder dykes for the shield stage are clustered in areas with expression as ridges below sea level (Orozco, 2016).

The shield unit (locally 'Punta Larga' and 'Puerto Inglés' sequences) is formed by basaltic, picrobasaltic and picritic lavas (Tables 2 and S.2, Fig. 3) with breccia layers and a few interbedded tephra horizons. The most common lithology carries olivine, plagioclase and clinopyroxene phenocrysts embedded in intersertal to intergranular groundmass (plagioclase, clinopyroxene, Fe-Ti oxides and rare olivine). Some rocks have abundant olivine (>20% vol, Table 1) with resorption rims in a subophitic groundmass. Vesicles are common (Table 1) and in some samples they are partially filled by a secondary mineralogy (mainly Fe-Ti oxides) also visible in glass. In some places this unit is characterized by the presence of basaltic dike swarms (Fig. 2a). A dike in the shield pile contains plagioclase-bearing dunite xenoliths that show a hetero-cumulate texture. Basaltic lava from the shield unit sampled at the present sea level gave an age of 3.83 ± 0.03 Ma ($^{40}Ar/^{39}Ar$ isochron in groundmass) (location in Fig. 1, data in Table S.1).

Rejuvenated volcanism is represented by the locally named 'Bahía del Padre' sequence, which fill the eroded morphology of the shield stage unit (Fig. 2b). This unit represents volcanic products erupted from minor eruptive centers, usually forming succesions of pyroclastic deposits that contain juvenile basanite material embedded in a yellow palagonitic matrix, covered by vesicle-poor (Table 1) basanite, and occasionally picrite (Tables 2 and S.2, Fig. 3) lava flows (~3 m thickness). Their mineralogy consists of olivine and zoned clinopyroxene phenocrysts with a groundmass that also contains plagioclase, Fe-Ti oxides, analcime and natrolite. Few samples show moderate alteration to Fe-Ti oxides in glass and veins. The $^{40}Ar/^{39}Ar$ age (step-heating in groundmass) of a basanite from this unit gave 0.90 ± 0.03 Ma (location in Fig. 1, data in Table S.1). Rocks from this unit rarely carry spinel lherzolite xenoliths that contain glassy vesicular veins with reaction rims around them.

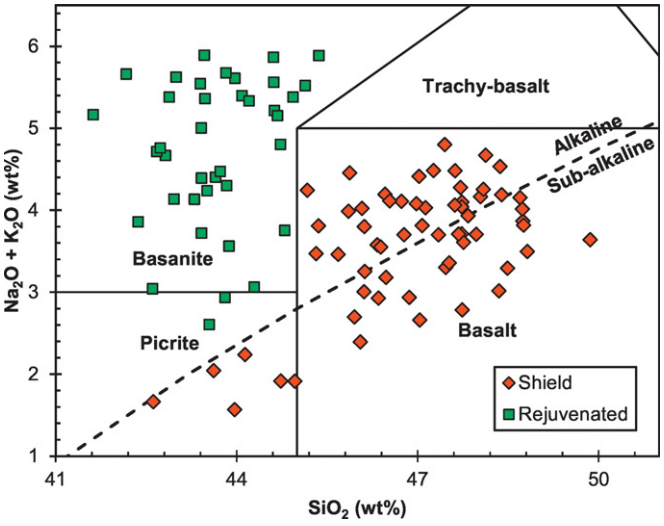

Fig. 3. Total-alkali vs. silica (TAS) classification diagram for the Robinson Crusoe Island lavas (after Le Maitre, 2002; alkali-subalkali boundary is from Irvine and Baragar, 1971). Previous data (Table S.2) from Gerlach et al. (1986); Baker et al. (1987) and Farley et al. (1993) are included.

4.2. Whole rock major element geochemistry

The shield unit contains transitional basalts, picrobasalts (Fig. 3) and picrites with SiO_2 contents ranging between 42.6 and 49.9 wt% (Tables 2 and S.2, all data normalized to 100%) and Mg-number (Mg# = $Mg^{2+}/[Mg^{2+}+Fe^{2+}]$ between 40.8 and 79.4 assuming 90% of total iron is ferrous in all samples (a reasonable estimate used in other oceanic islands like Hawaii, e.g., Garcia, 1996). Based on Mg#, Ni, and olivine content the shield lavas are grouped in: (1) 'differentiated' basalts (Mg# < 58.1, Ni < 111 ppm, low olivine); (2) primitive or 'near primitive' basalts (59.7 < Mg# < 68.1, 158 < Ni < 266 ppm, high olivine); (3) 'olivine-rich' basalts, similar to 'masafuerites' as defined by Quensel (1920) in Alexander Selkirk island (Mg# > 69.4, Ni > 514 ppm, very abundant olivine) (Fig. 4). Some chemical differences arise between these groups: the 'differentiated' group displays the highest contents of TiO_2, Al_2O_3 and CaO (3.1–4.4/13.9–16.6/8.2–12.9 wt%) with classical characteristics of fractional crystallization (e.g., clinopyroxene) (Fig. 5); the 'olivine-rich' group shows the lowest values (1.6–3.1/6.5–11.4/5.0–9.3 wt%) as a result of olivine accumulation (Fig. 5); and the 'near-primitive' group covers an intermediate range (2.5–3.4/12.1–14.9/7.2–13.1 wt%) (Fig. 5), probably due to

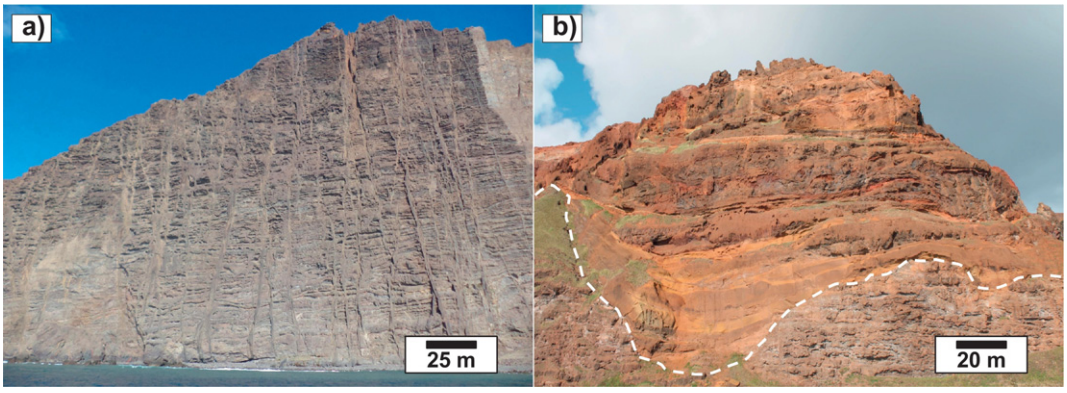

Fig. 2. Field photographs of Robinson Crusoe Island. a) Basaltic dike swarms in the shield unit (located in Puerto Inglés, Robinson Crusoe Island). b) A pile representing the rejuvenated volcanism (~0.90 Ma) filling with unconformity (dashed line) the eroded morphology of the shield unit (~3.83 Ma, NW of Puerto Francés).

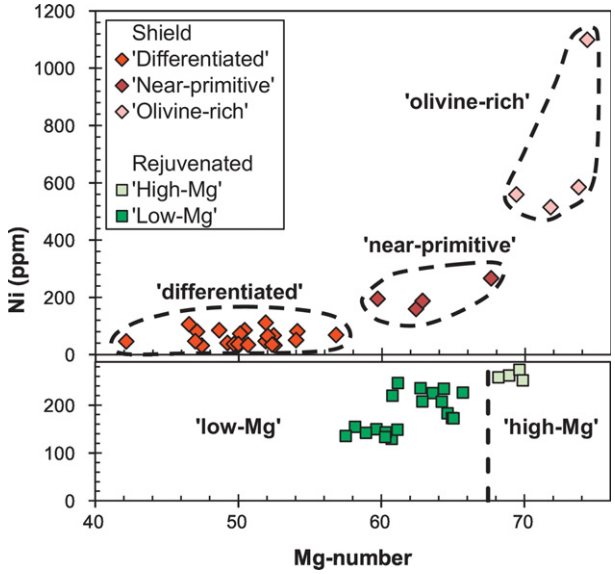

Fig. 4. Mg# vs. Ni content diagram and compositional classification of shield and rejuvenated lavas from Robinson Crusoe Island. Only high-precision Ni data (ICP-MS) are included (previous work data excluded).

mixing between primitive (high-T) and differentiated melts (low-T) as suggested by Natland (2003). Variations in mobile elements (as Na_2O in Fig. 5) can be explained as an effect of alteration. These groups do not have a clear geographic or stratigraphic distribution.

The rejuvenated unit is composed by basanite and picrite lavas (Fig. 3). Their SiO_2 and Mg# contents range between 41.6 and 45.4 wt% (Tables 2 and S.2) and 55.9–69.9, respectively. Other remarkable compositional differences (major elements) between the units are visible in the MnO (shield/rejuvenated ratio: 0.12–0.20/0.19–0.24 wt%), Na_2O (1.3–3.5/1.8–4.7 wt%) (Fig. 5, K_2O (0.05–1.35/0.54–2.17 wt%) and P_2O_5 (0.18–0.65/0.45–0.97 wt%) content (Na_2O and P_2O_5 in Fig. 5). These differences would be explained by changes in the source and/or variations in degree of partial melting, although a detailed analysis of the source is beyond the scope of this study. According to their major elements geochemistry and Mg#, two compositional groups can be established in this unit: a 'high-Mg' group formed by primitive lavas (Mg# > 68), and a 'low-Mg' group with slightly differentiated basanites (Fig. 4). Other chemical differences between both groups are subtle, and only slight differences in the Fe_2O_3, MnO and P_2O_5 contents are appreciable. In fact, the 'low-Mg' shows the highest values of these oxides (Fe_2O_3: 12.1–15.0/MnO: 0.20–0.24/P_2O_5: 0.57–0.97 wt%) compared to the 'high-Mg' group (12.1–13.6/0.19–0.20/0.45–0.69 wt%) (P_2O_5 in Fig. 5). Internal variations in rejuvenated lavas can be thus related to fractional crystallization (olivine and clinopyroxene), magmatic recharge (generating some mixing) or alteration (in mobile elements).

4.3. Mineral chemistry and geothermobarometry

4.3.1. Methodology

Pressure conditions were estimated using clinopyroxene EPMA data and the structural geobarometer of Nimis and Ulmer (1998) for anhydrous basalts. The standard error of this method (anhydrous basalts) is ±1.7 kbar, but the presence of water in the system increases the pressure in ~1.0 kbar per 1 wt% H_2O content. Only for reference, according to their Ce content, parental magmas in Juan Fernández Ridge would have 0.8–1.0 wt% H_2O in the shield stage, and 1.5–2.0 wt% in rejuvenated volcanism (Dixon et al. (2002) as estimated for Pacific FOZO magmas [H_2O/Ce = 200]). The possible presence of water increases the error, but we prefer this method instead of Nimis and Ulmer (1998) for hydrous basalts, Nimis (1999), Putirka et al. (2003) and Putirka (2008a), which need clinopyroxene temperature estimation. The latter is difficult to obtain without orthopyroxene, and/or liquid-crystal equilibrium, absent in most samples of Robinson Crusoe Island, especially in rejuvenated magmas, considering $^{Cpx\text{-}Liq}Kd$ value ($^{Cpx\text{-}Liq}Kd = X^{Oliv}_{FeO} * X^{Liq}_{MgO} / X^{Liq}_{FeO} * X^{Oliv}_{MgO}$) of 0.27 ± 0.03 representative of equilibrium conditions (e.g., Putirka et

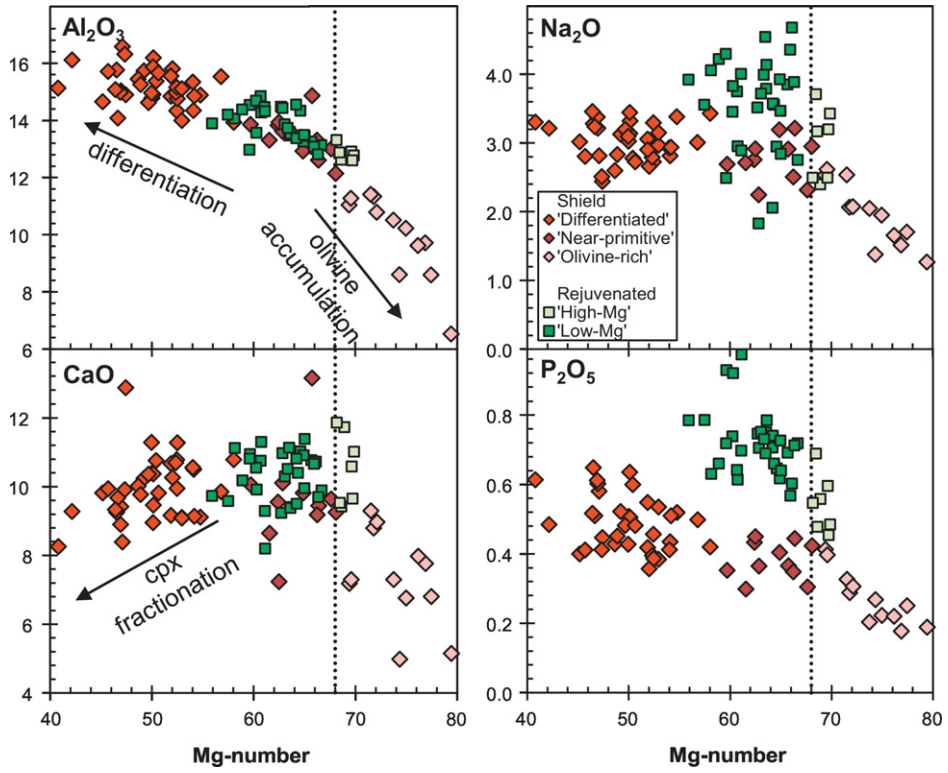

Fig. 5. Mg# variations vs. major elements (Al_2O_3, Na_2O, CaO and P_2O_5 in wt%) plots for lavas from Robinson Crusoe Island. Dashed line indicates possible primitive compositions (Mg# > 68).

al., 2003) (Table S.3). We do not use olivine-liquid temperatures as input of T-dependent geobarometers because they cannot be assumed as clinopyroxene temperatures. Given the high error of the method, the results are relevant from a qualitative point of view, as they represent major trends in a group of samples, or significant variations in individual crystals. A pressure estimate of 0.0 kbar (or slightly <0.0 kbar) represents shallow conditions of crystallization (Nimis, 2014 in ResearchGate web). Structural formula and Fe^{3+} contents for clinopyroxene were calculated through charge balance (Papike et al., 1974) according to the methodology by Nimis and Ulmer (1998) (CpxBar software). Wollastonite content (Wo) was calculated as Wo = 100*(Ca/[Ca + Mg + Fe]), where Mg and Fe are molar concentrations.

Crystallization temperatures were estimated using the olivine-liquid geothermometer of Herzberg and O'Hara (2002) modified from Beattie (1993). Their standard error is ±31 °C. Olivine composition was measured by EPMA and major elements geochemistry were considered as representative of the liquid composition (we used only phenocrysts-poor samples: <13 vol% considering also microphenocrysts, see Table 1). Canonical $^{Ol\text{-}Liq}Kd$ values ($^{Ol\text{-}Liq}Kd = X^{Oliv}_{FeO} * X^{Liq}_{MgO} / X^{Liq}_{FeO} * X^{Oliv}_{MgO}$) of 0.30 ± 0.03 were considered in olivine-liquid equilibrium (Roeder and Emslie, 1970) (Fig. 6). Given the estimated pressures for the shield and rejuvenated magmas (Table 3, described in Sections 4.3.2 and 4.3.3), and in order to make valid comparisons, we fix the pressure value as input for geothermometer in 2.0 kbar for all units, which is the most frequent value obtained (excluding values near to 0.0 that represent shallow crystallization, see histograms in Fig. 11). Note that a pressure increase of 1.0 kbar generates an increase of ~5 °C in the temperature estimation. All Fe in olivine is considered as Fe^{2+} and forsterite content (Fo) was calculated as Fo = 100*(Mg/[Mg + Fe^{2+}]), where Mg and Fe are molar concentrations. For the shield stage we also estimated clinopyroxene-liquid temperatures (2σ standard deviation of ±33 °C) considering $^{Cpx\text{-}Liq}Kd$ values 0.24–0.30 representative of equilibrium conditions (Putirka et al., 2003) using the pressure from Nimis and Ulmer (1998) anhydrous basalts as input.

4.3.2. Pressure and temperature for the shield stage

Clinopyroxene is common in the shield lavas, although not always as phenocryst in all samples. Usually they are eu- to subhedral homogeneous crystals, isolated or in a glomeroporphiric texture with olivine and plagioclase. In general, their diameter is <0.7 mm with a variable composition in the range of $Wo_{42-47}En_{39-48}Fs_{8-17}$, Na_2O : 0.16–0.54 and TiO_2 : 0.80–3.61 wt% (Fig. 7 and Table S.3). Clinopyroxene composition is the same in 'differentiated', 'near-primitive' and 'olivine-rich' groups. Pressure conditions estimated for the shield lavas are 0.0–3.2 kbar (Table 3, most samples between 1.0 and 2.0 kbar, see histogram in Fig. 11). The latter also supports the choice of pressure input of 2.0 kbar for olivine-liquid geothermometer.

Table 3
Pressure and temperature calculated from clinopyroxene and olivine crystals from Robinson Crusoe Island, n indicates the number of samples considered in each compositional group.

Geological unit	Compositional group	n	Cpx_{an} P (kbar)[A]	n	Ol-Liq T (°C)[B]	n	Cpx-Liq T (°C)[C]
Shield	Olivine-rich		–		–		–
	Near-primitive	2	0.0–2.9	1	1321	1	1205–1221
	Differentiated	7	0.0–3.2	2	1156–1181	5	1162–1194
Rejuvenated	High-Mg	2	0.0–3.7	2	1316–1354		–
	Low-Mg	5	0.0–10.8	3	1256–1295		–

[A] Clinopyroxene pressure in anhydrous basalts from Nimis and Ulmer, 1998 (±1.7 kbar + ca. 1 kbar per 1 wt% H_2O in melt).
[B] Olivine-liquid temperature from Herzberg and O'Hara, 2002 (±31 °C).
[C] Clinopyroxene-liquid temperature from Putirka et al., 2003 (±33 °C).

The olivine phenocrysts in the shield unit are eu- to subhedral, with diameter up to 1.8 mm with an iddingsite altered rim (Fig. 8a) (of variable width, sometimes obliterating the whole crystal). Their chemical composition ranges between Fo_{76-88} and Ni : 196–2695 ppm commonly with normal zonation (Figs. 8a and 10a). In the 'olivine-rich' and 'near-primitive' groups there is an abundance of high Fo values (Fo_{84-88}) (Table S.4). Estimates of crystallization temperature in one sample of 'near-primitive' group are 1321 °C (Tables 3 and S.4), but the analyzed lava of 'olivine-rich' group do not show chemical equilibrium with liquid (Fig. 6). In the 'differentiated' group some rims of zoned crystals

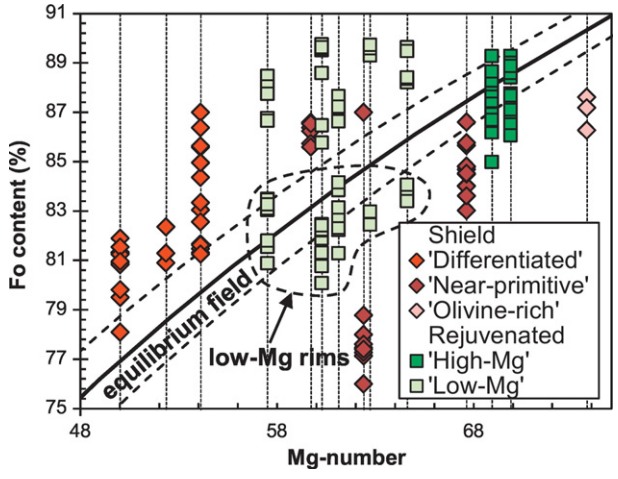

Fig. 6. Olivine Fo content vs. whole-rock Mg# for Robinson Crusoe Island lavas. Olivine-liquid equilibrium field after Roeder and Emslie (1970) using a $^{Ol\text{-}Liq}Kd$ of 0.30 ± 0.03.

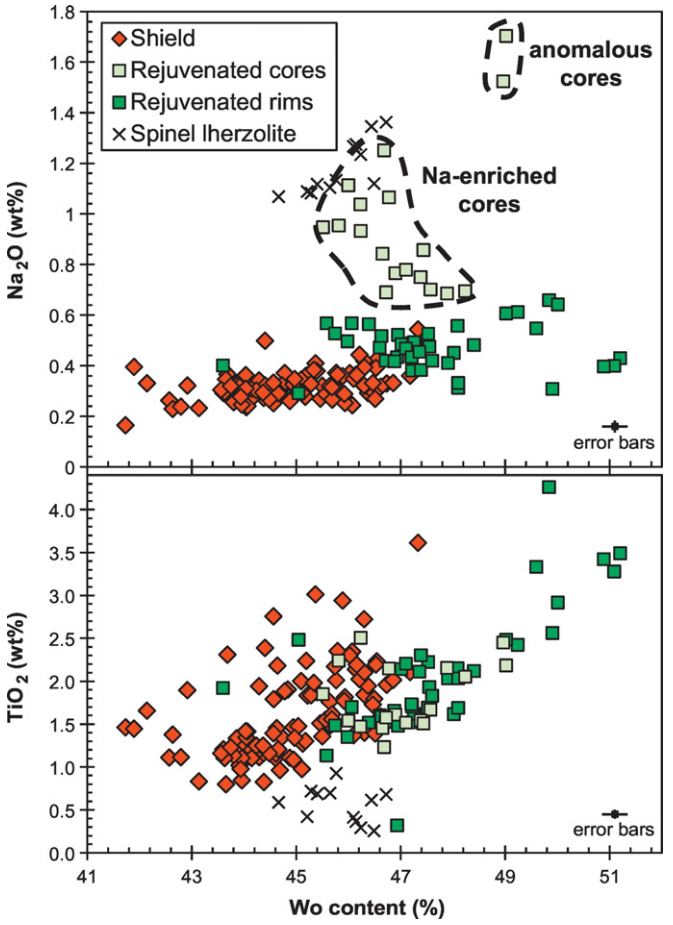

Fig. 7. Clinopyroxene composition, Na_2O and TiO_2(wt%) vs. Wo content in Robinson Crusoe Island. Dashed lines enclose 'low-Mg' cores compositions (described in text). Spinel lherzolite xenoliths data is also included showing differences respect to rejuvenated (Na-enriched) cores that suggest differences in their origin. Error bars reflect the mean of the SD(%) values reported by microprobe.

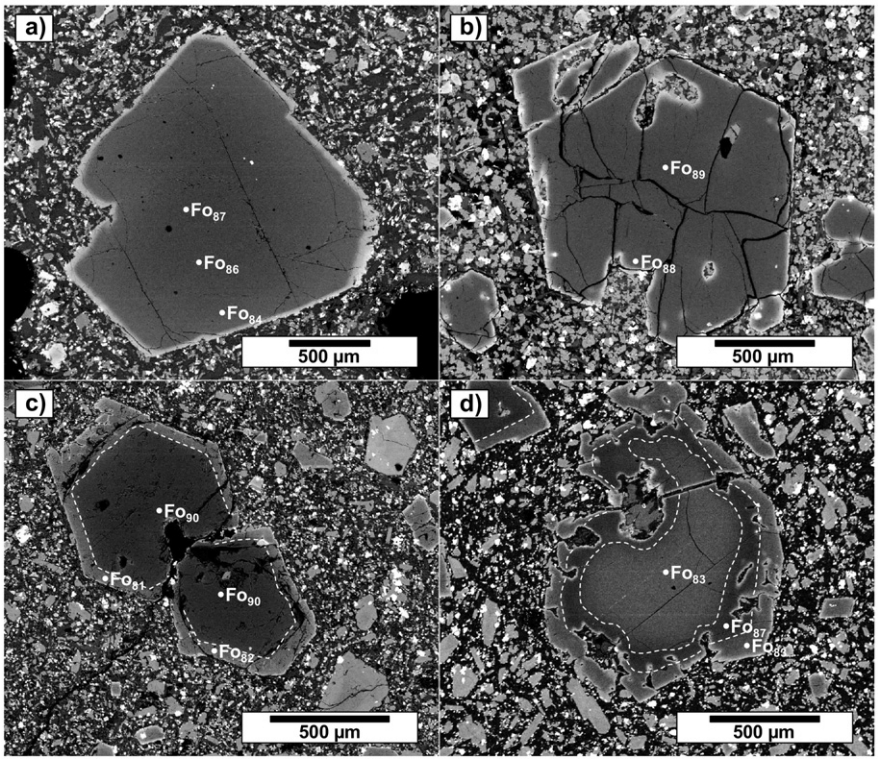

Fig. 8. SEM microphotographs of olivine. Fo content is indicated. a) Typical phenocryst with normal zonation of 'differentiated' group in shield unit. b) High-Fo compositions of 'high-Mg' group in rejuvenated unit. c) Classical 'low-Mg' group pattern: high-Fo cores (antecrysts) and differentiated rims in the rejuvenated unit. d) Anomalous cores (xenocrysts) in rejuvenated unit surrounded by typical 'low-Mg' compositions (described in c).

are in textural and chemical equilibrium with liquid (Fig. 6) giving temperatures in the range 1156–1181 °C (Tables 3 and S.4). Olivine-liquid temperature of the 'differentiated' lavas are well correlated with those obtained by the clinopyroxene-liquid equilibrium geothermometer, which varies between 1162 and 1194 °C (Tables 3 and S.3). This does not occur in 'near-primitive' group where clinopyroxene-liquid temperature is 1205–1221 °C (Tables 3 and S.3) (but in a sample with Mg# of 59.7 in contrast of 67.6 in the sample measured with olivine-liquid geothermometer).

4.3.3. Pressure and temperature for the rejuvenated stage

The rejuvenated lavas contain clinopyroxene as a ubiquitous phase, generally visible as phenocrysts (up to 1.6 mm in diameter) and in the groundmass. The main compositional differences respect to shield unit are the higher contents of Wo component and Na_2O (Fig. 7 and Table S.3). According to their mineral chemistry and pressure estimation, the 'high-Mg' and 'low-Mg' groups can be analyzed separately.

The 'high-Mg' group is characterized by the presence of subhedral microphenocrysts of clinopyroxene with diameter <0.3 mm. Generally they exhibit oscillatory zonation and have compositions in the range of $Wo_{44-51}En_{36-44}Fs_{8-17}$, Na_2O: 0.29–0.64 and TiO_2: 1.69–3.49 wt% (Table S.3). Resorption rims are absent and their crystallization pressure was estimated between 0 and 3.7 kbar (Table 3 and S.3). On the other hand, the 'low-Mg' group shows a more complex compositional and textural pattern. In general, Na-enriched cores (<1.1 mm in diameter) are visible with composition in the range of $Wo_{46-48}En_{38-45}Fs_{8-15}$, Na_2O: 0.69–1.25 and TiO_2: 1.23–2.51 wt% (Fig. 7) that usually show evidences of resorption (sinuous and irregular rims), without zonation and occasionally 'spongy' texture. The formation pressure of these Na-enriched clinopyroxene cores was estimated in the range 3.7–10.8 kbar (Table S.3) (most of the estimates are >5.0 kbar, see histogram in Fig. 11), the highest values for Robinson Crusoe Island lavas. Around the cores there are rims (<0.25 mm in diameter) that develop oscillatory zonation with chemical ($Wo_{46-50}En_{34-48}Fs_{5-16}$, Na_2O: 0.38–0.66 and TiO_2: 0.32–4.26 wt%) and textural characteristics very similar to the 'high-Mg' clinopyroxenes (Fig. 7). The pressure estimated for the rims was 0–5.2 kbar (Table S.3) (most of the data <3.0 kbar, see histogram in Fig. 11) generating important variations (e.g., 1.7–10.3 kbar) in single crystals from the 'low-Mg' group (Fig. 9a). Compositional outliers (in clinopyroxene crystals with notable resorption rims) are scarcely recognizable in one sample of the 'low-Mg' group, with diameter <0.6 mm and $Wo_{49}En_{30-31}Fs_{20-21}$, Na_2O: 1.52–1.70 and TiO_2: 2.19–2.45 wt% (Figs. 7 and 9b), but their pressure conditions cannot be estimated because of the low Mg# of the crystals for the Nimis and Ulmer (1998) geobarometer. Then, the rejuvenated volcanism is characterized by the formation of clinopyroxene with high-pressure Na-rich cores (only in 'low-Mg' group and occasionally around anomalous compositions) followed by low-pressure rims (in both groups).

Olivine is a ubiquitous phenocryst in lavas of the rejuvenated volcanism, with diameter up to 4.0 mm and a notably thinner iddingsite rim than those from the shield unit. They are characterized by the presence of Mg-rich cores (<1.6 mm in diameter, Fo_{85-90}, most of the samples around Fo_{88} and Ni: 534–2617 ppm) (Fig. 10a and Table S.4) sometimes in equilibrium with the mantle and melts derived from it (Fo > 88). Mg-rich cores compose the whole crystals in the 'high-Mg' group (Fig. 8b) and are in chemical and textural equilibrium with the liquid (Fig. 6). This allow us to estimate the olivine-liquid equilibrium temperature for the 'high-Mg' group between 1316 and 1354 °C (Tables 3 and S.4), the highest values in Robinson Crusoe Island. But in the 'low-Mg' group, the Mg-rich cores show resorption rims with chemical disequilibrium (Table S.4) and are surrounded by more differentiated rims (diameter < 0.1 mm, Fo_{80-84}, Ni: ~0–1658 ppm) (Fig. 8c) in equilibrium with the liquid (Fig. 6). Then, the temperature for the 'low-Mg' group was estimated in the range 1256–1295 °C (Tables 3 and S.4). Some olivines from both groups have cores with anomalous compositions (different to Mg-rich cores) that can be interpreted as xenocrysts remnants. Most of olivine xenocrysts are characterized by low Ca (<700 ppm) and high Fo_{84-90} contents (Fig. 10b) and might be

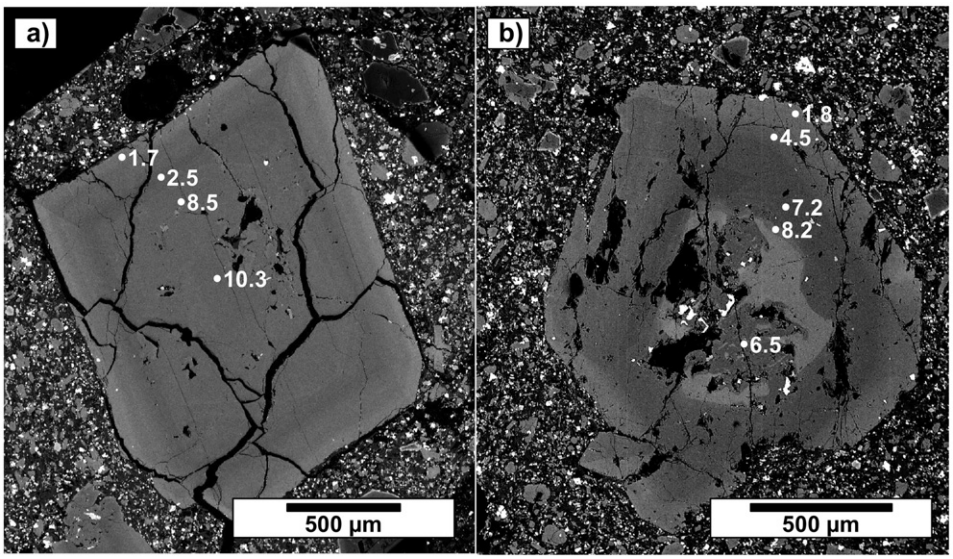

Fig. 9. SEM microphotographs of clinopyroxene in rejuvenated lavas. Pressure estimations (kbar) are indicated. a) Classical pattern in 'low-Mg' group: Na-enriched cores (antecrysts formed at high-pressure) with polybaric crystallization and more differentiated rims (low-pressure phenocrysts). b) Na-enriched cores (antecrysts) and differentiated rims (phenocrysts) surrounding anomalous cores (unknown origin xenocrysts) with resorption rims in one sample of 'low-Mg' group.

interpreted as mantle olivines (discussed in Section 5.1). These olivines do not display significant differences respect to the typical Mg-rich cores of the rejuvenated unit, which make them indistinguishable in absence of EPMA data. In the 'high-Mg' group these xenocrysts are in chemical and textural equilibrium with the liquid (Table S.4), but in the 'low-Mg' group they show resorption evidences and are surrounded by the characteristic $Fo_{80–84}$ rims. Another set of xenocrysts is scarcely visible only in the 'low-Mg' group. These correspond to the lowest values of Fo in the rejuvenated unit ($Fo_{78–84}$) with crystals showing notable resorption rims. The classical pattern of 'low-Mg' olivine (Mg-rich cores and differentiated rims) is visible around these anomalous xenocrysts (Fig. 8d). In summary, the olivine evolution consist in the formation on Mg-rich cores ($Fo_{85–90}$, T: 1316–1354 °C), occasionally around xenocrysts ($Fo_{84–90}$ or $Fo_{78–84}$) (in both groups), surrounded by more differentiated rims ($Fo_{80–84}$, T: 1256–1295 °C) only in the 'low-Mg' group.

4.3.4. Xenoliths

Plagioclase-bearing dunite xenoliths are recognized in a dyke of the rejuvenated unit with hetero-cumulate texture that suggests their origin from cumulated ultramafic intrusive. In fact, their mineralogy (see Table 1) (plagioclase presence implies shallow crystallization) and olivine chemistry (Fo < 82.7, Ni < ~2000 ppm and Ca > 1000 ppm) (Table S.4) discard a mantle origin. Olivines are very similar to those from shield stage lavas, which suggest that xenoliths are carried out from intrusive bodies probably formed by olivine accumulation from shield-like magmas. In the rejuvenated unit it is also possible to recognize xenolithic fragments that consist of spinel lherzolites in basanite dykes and lavas. Their mineralogical (Table 1) and textural characteristics (e.g., glass veins and reaction rims on minerals in contact with them) admit an origin in the mantle. The olivine chemistry ($Fo_{88–89}$, Ni > 2200 ppm and Ca < 650 ppm) (Table S.4) confirms their mantle origin (e.g., Simkin and Smith, 1970). Pressure conditions in clinopyroxene were estimated between 8.9 and 11.0 kbar (Table S.3) (Nimis and Ulmer, 1998), depth associated with lithospheric mantle (i.e., > ~ 32 km depth).

5. Discussion

5.1. Heterogeneous crystal origin

Clinopyroxenes and olivines in the shield lavas show compositional features interpretable as phenocrysts origin (defined as phases that are in equilibrium with the liquid), crystallized from a liquid affected by shallow fractional crystallization (Fig. 10a). The possibility that the cores in zoned crystal correspond to antecrysts (defined as crystals that did not crystallized directly from the host melt but maintain a genetic relationship with the same system; e.g., Davidson et al., 2007) is plausible but difficult to confirm. According to the olivine Fo and Ni content (Fig. 10a), the shield magmatism has an origin in a peridotitic source probably similar to Hawaiian tholeiitic melt source (based on crystallization trend from Wang and Gaetani, 2008). Minor participation of pyroxenite (according to a crystallization trend from peridotite and pyroxenite source from Ruprecth and Plank, 2013) cannot be discarded but olivines from the shield stage do not show classical features considered as pyroxenite signature (e.g., high contents of Ni, after Sobolev et al., 2005). Although Herzberg and O'Hara (2002) geothermometer was calibrated in primary magmas from peridotite source, they discussed that the presence of pyroxenite/eclogite is a problem only if they exist as a distinct lithology (e.g., as veins) and not as source of chemical metasomatism. We do not have evidences of pyroxenite/eclogite veins in Robinson Crusoe.

In the rejuvenated lavas there are clinopyroxenes cores with chemical compositions interpretable as phenocrysts, xenocrysts or antecrysts crystallized at different conditions. An important feature of the clinopyroxenes in the 'low-Mg' group is the presence of Na-rich cores that yields the higher pressures estimates, which could be interpreted as an origin in the mantle. However, from a comparison with mantle clinopyroxenes (data from spinel lherzolites as xenoliths in 'low-Mg' group) notable differences arise, (e.g., TiO_2, Al_2O_3 and Cr_2O_3 contents) (TiO_2 in Fig. 7), which suggests that Na-rich cores are not evident mantle xenocrysts. In addition, Robinson Crusoe lavas do not show any composition similar to these Na-rich cores, which allow us to discard them to be considered as xenocrysts originated at shield stage. We interpret these Na-rich clinopyroxene cores as antecrysts and the chemical differences as a result of crystallization from a liquid more primitive than the rims-equilibrated melts, which explain their presence only in 'low-Mg' group (no primitive compositions). Same situation has been observed in rocks of other oceanic islands, e.g., the post-shield lavas at Hawaii (Welsch et al., 2016). Only the Na-rich cores formed at pressures ~10 kbar could be mantle xenocrysts (those chemically similar to spinel lherzolites). Rare cores highly enriched in FeO^T and Na_2O in one sample of 'low-Mg' group are considered xenocrysts of

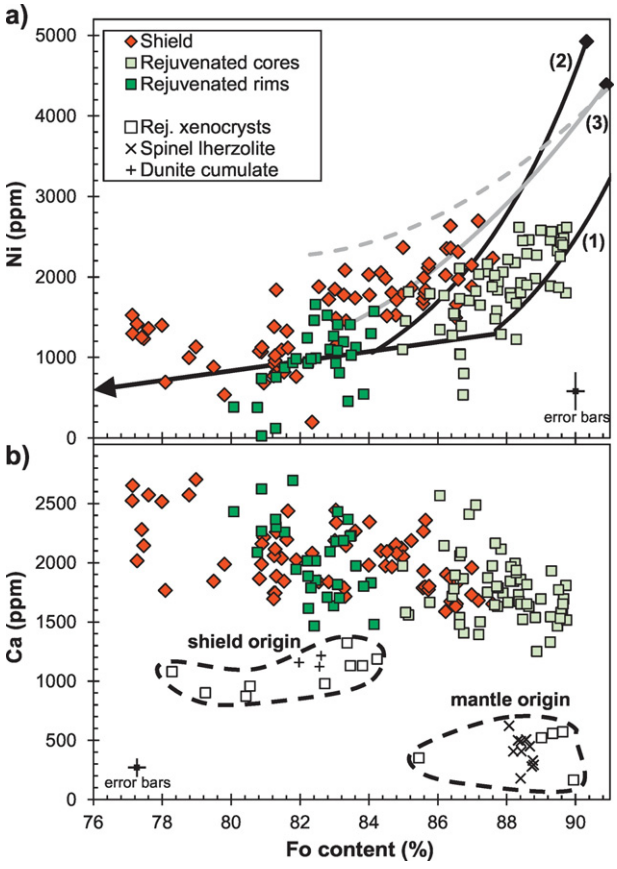

Fig. 10. Olivine composition in Robinson Crusoe Island. a) Ni (ppm) vs. Fo content. Crystallization trends for different primary melts are provided: (1) and (2) fractional of primitive magma from peridotite and pyroxenite source respectively, arrow indicates shallow crystallization trend (Rupreth and Plank, 2013; sources from Straub et al., 2011), (3) batch (dashed line) and fractional (solid line) of primitive Hawaiian tholeiitic melt without eclogite partial melt (Wang and Gaetani, 2008). b) Ca (ppm) vs. Fo content, spinel lherzolite and dunite cumulate data is showed and allows to interpret the origin of rejuvenated xenocrysts (dashed curves enclose mantle or shield-like compositions). Error bars reflect the mean of the SD(%) values reported by microprobe.

enigmatic origin due to their anomalous composition (Fig. 7), different to any composition (lavas, dunite or lherzolite) in Robinson Crusoe Island.

The olivines from the rejuvenated magmas show cores with different compositions (up to three in one sample). Most of them are formed directly from magmas in equilibrium (or near-equilibrium) with the mantle (according their Fo and Ca content) and correspond to phenocrysts in 'high-Mg' group and antecrysts in 'low-Mg' lavas. According to their chemical composition they come from a peridotitic source, apparently with minor or null participation of pyroxenite or eclogite derived melts (Fig. 10a). Two sets of cores have an enigmatic origin. The first one has major element geochemistry identical to phenocrysts ($Fo_{84–90}$) but strong variations in some trace elements (Ni > 2000 ppm and Ca < 700 ppm). These features have been assigned to mantle olivines (e.g., Simkin and Smith, 1970; Boudier, 1991; Hirano et al., 2004; Rohrbach et al., 2005). However, recent studies indicate that such compositions may also be generated from non-mantle conditions (e.g., Kamenetsky et al., 2006; Li et al., 2012). In this case, the remarkable compositional similarity of these crystals with olivines from spinel lherzolites (mantle xenoliths) (Fig. 10b) allows to interpret their origin as mantle xenocrysts. The second set has the lowest Fo values of the rejuvenated unit ($Fo_{78–84}$ and Ca > 800 ppm) and shows evident chemical similarities with olivines of dunite cumulates in the shield unit (Fig. 10b). Then, their origin is interpreted as xenocrysts from shield-like magmas.

The rims of olivine and clinopyroxene are in textural (and chemical for olivines, Fig. 6) equilibrium with the liquid and we interpret that they are formed directly from the magma as phenocrysts. The evolution trend of both mineral rims follows the classic shallow fractional crystallization trend (Fig. 10a for olivine).

5.2. Contrasting magma ascent and storage paths

5.2.1. Shield volcanism

The estimated pressure-temperature pre-eruptive conditions for the shield volcanism, their chemical features (abundant differentiated and cumulated rocks) and xenolith content (only from shallow origin) allow us to infer the existence of shallow magmatic reservoirs, where the ascending magmas would have been stored, crystallized and sometimes differentiated. These reservoirs were located at depth between ~3 and 11 km (1–3 kbar, Fig. 11), and probably had a considerable size due to the volume of erupted material. Inside of this shallow reservoir the three types of magmas defined for the shield stage resided, but undergone a different evolutionary history. The 'differentiated' group is formed by magmas that were stored and differentiated in the reservoir (shallow fractional crystallization and magmatic recharge). During the chamber evolution the magmatic differentiation would have caused a significant temperature decrease to ~1156–1181 °C. These temperatures are well correlated with Kilauea geothermometer (Helz and Thornber, 1987) estimations of Natland (2003). This group represents the largest volume of magma erupted in Robinson Crusoe Island.

The 'near-primitive' group is composed by basaltic magmas with high content of olivine that undergone little (or no) differentiation and were partially mixed with magmas from the 'differentiated' group. Their olivines were formed at ~1321 °C and thus the whole rock chemistry closely reflects the primitive composition of the shield magmatism in Robinson Crusoe Island. Differences in the degree of magma mixing explain the clinopyroxene-liquid temperatures of 1205–1221 obtained in a more evolved sample of this group. Natland (2003) also recognized the mixing processes between cold magmas and hotter olivine-bearing magmas.

Finally, we interpret the formation of the 'olivine-rich' group as a result of fractional crystallization and gravitational settling in the reservoir or pick-up of primitive antecrysts. The olivine accumulation also explains the formation of plagioclase-bearing dunites cumulates at shallow conditions carried in one dyke of the shield unit.

Putirka (2008b) estimated an average olivine-liquid temperature of 1517 °C for primitive magmas in Juan Fernández Ridge. We cannot evaluate this estimation because samples details were not provided (taken from GEOROC database that contains both shield and rejuvenated samples together with olivine-cumulated rocks).

5.2.2. Rejuvenated volcanism

Magma ascent and storage conditions for the rejuvenated volcanism are different when compared to the shield stage. Fractional crystallization in shallow reservoirs was replaced by high-pressure crystallization, direct ascent and only occasional short-time storage in low-volume reservoirs (Fig. 11).

Basanites of 'high-Mg' group represent primitive magmas in equilibrium with the mantle. Clinopyroxene began to crystallize at shallow depth < 15 km (<4 kbar) without evidence of polybaric ascent (absence of high-pressure cores and chemical signs of fractionation). Olivine was formed at temperatures about 1316–1354 °C, probably starting from deep regions ~33–41 km (9–11 kbar) where xenocrysts were captured (only distinguishable by trace elements). There is no evidence of storage in shallow reservoirs for this group.

For the 'low-Mg' group we interpret a complex storage and ascent history. First, xenocrysts of olivine and lherzolite xenoliths were incorporated at ~33–41 km depth (9–11 kbar). Probably a coeval polybaric crystallization of high-pressure clinopyroxene started at ~40 km ending at ~18 km (~5–11 kbar, with a few cases at ~13 km or ~3.5 kbar). After

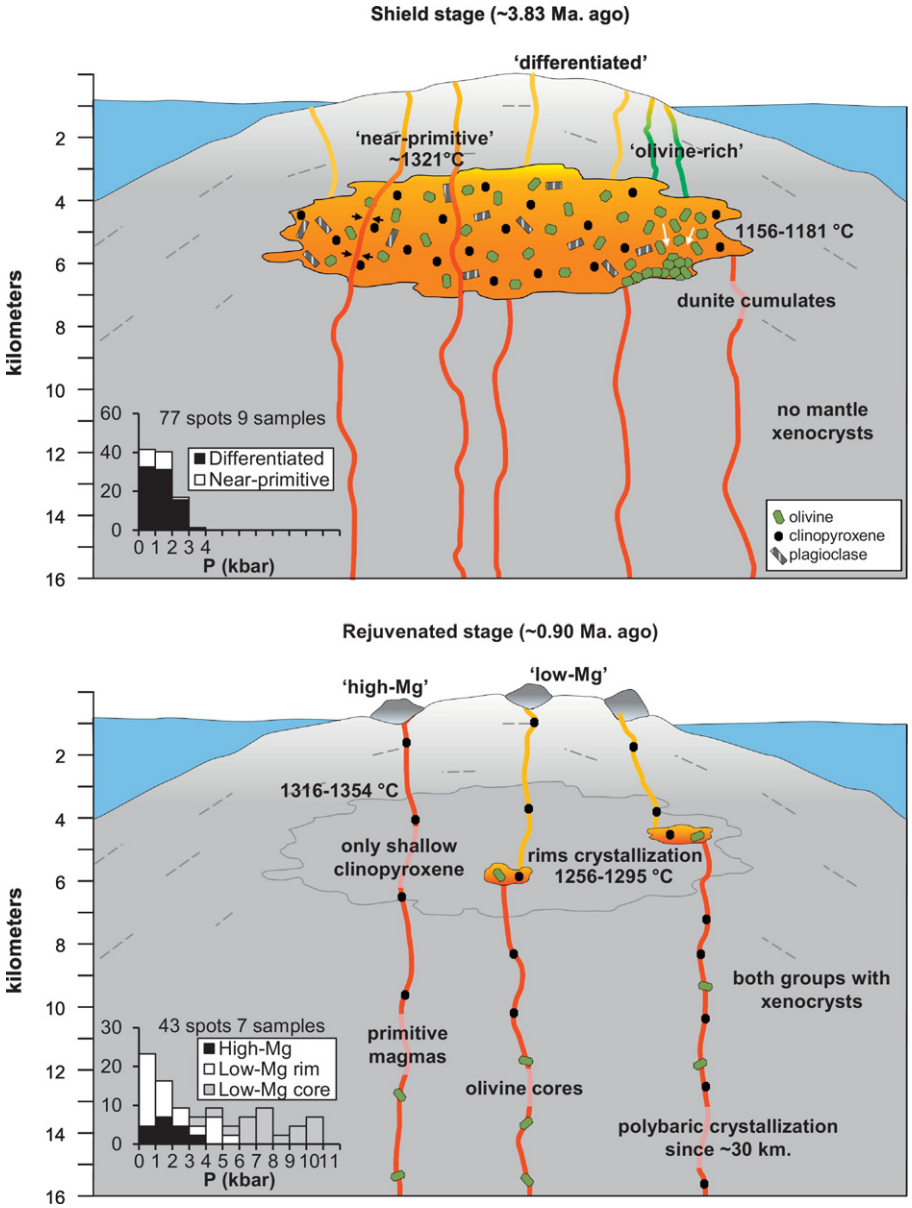

Fig. 11. Schematic model of the magmatic ascent and storage in Robinson Crusoe Island showing the contrasting pattern for shield and rejuvenated volcanism: storage in shallow reservoirs for shield and rapid ascent with polybaric crystallization for the rejuvenated stage (details in Section 5.2). Qualitative differences in depth (from pressure estimations of clinopyroxene geobarometer from Nimis and Ulmer, 1998) and temperature conditions (according olivine-liquid geothermometer from Herzberg and O'Hara, 2002) of each compositional group are also shown. Pressure conditions estimated are showed in histograms for both units.

that, magmas ascended quickly (preserving xenoliths) and formed resorption rims in the cores (probably due to magma mixing or recharge that changed the magma chemistry). Finally we suggest the magma storage occurred at low-volume shallow reservoirs (depth < ~18 km or ~5 kbar) where the rims of both olivine and clinoyroxene formed at temperatures between ~1256–1295 °C. The preservation of zonation in olivine (preventing elemental diffusion) suggests short-time residence in the reservoir (e.g., Ruprecth and Plank, 2013).

5.3. Robinson Crusoe storage system in hotspot global view

Our model suggests the existence of shallow reservoirs at the shield stage in Robinson Crusoe (<10 km, Fig. 11). Similar models have been proposed for other oceanic islands using different techniques. Based on geophysical data (Ryan, 1988; Poland et al., 2014; Tilling et al., 2014), geochemical-geological observations (Clague, 1987) and high-precision Pb isotope analysis (Pietruszka et al., 2015), one or several shallow magma reservoirs (<7 km depth) have been recognized for the shield stage in Hawaii. In addition, for Réunion shield stage Fisk et al. (1988) identified reservoirs between 5 and 8 kbar (from melting and recrystallization experiments at pressure from 1 atm to 20 kbar) and Peltier et al. (2009) proposed storage regions at 2.3, 7.5 and 15 km based on geophysical data. These data support the idea that shield stage volcanism is fueled from shallow magmatic reservoirs.

For rejuvenated volcanism in Hawaii, Clague (1987) proposed the absence of shallow or intermediate reservoirs based on xenoliths occurrence and chemical primitive features of the alkaline magmas. Rejuvenated magmas in Robinson Crusoe bring also mantle xenoliths (spinel lherzolite) with primitive chemistry (confirmed by Mg# and olivine-liquid temperatures), and our pressure estimations indicate a deep origin (within the mantle). Similar conditions have been proposed for other alkaline rocks from oceanic islands. For Hawaii postshield stage, Chatterjee et al. (2005) identified reservoirs in the mantle and Hammer et al. (2016) recognized crystallization in mantle conditions,

although some shallow reservoirs in crustal levels as well. High depths (within the mantle) up to 9.5 kbar have also been estimated for the reservoir of postshield alkali rocks from Canary Islands (Hansteen et al., 1998).

Thus, shallow reservoirs for shield stage and deeper P conditions for rejuvenated volcanism seem to be a global pattern, despite the regional geodynamical features that control long-term evolution of hotspot volcanoes.

6. Conclusions

Contrasting patterns of ascent and storage have been recognized for shield and rejuvenated volcanism in Robinson Crusoe Island, a classical example of intraplate magmatism fed by a primary mantle plume. In fact, whole rock and mineral chemistry (P-T estimations) allow us to infer shallow storage conditions (~3–11 km) for the shield stage (dated in ~3.83 Ma) and rapid ascent with polybaric crystallization (started at ~40 km) for the rejuvenated stage (dated ~0.90 Ma). Shallow (and probably large) magma chambers during the shield stage control the low-pressure differentiation and might be responsible for the high growing rate of the central volcano now represented by the ca. 2000 thick volcanic pile and related dyke swarms. On the other hand, direct ascent of small magma batches extracted during the rejuvenated stage well explains the distributed occurrence of minor eruptive centers feeding low volume eruptions. These findings provide a framework for the long-term volcanic evolution of the island and point to a characteristic behavior also proposed in other oceanic islands as Hawaii or Réunion.

Acknowledgments

This research was supported by FONDECYT 1110966, 1141303 (both granted to L. E. Lara) and FONDAP 15090013 projects. Main results presented in this manuscript are part of the first author's doctoral thesis also supported by a CONICYT fellowship. Authors are grateful to Michael Garcia and Jasper Konter for providing constructive reviews that improved this paper. We also acknowledge LAMARX – Universidad Nacional de Córdoba staff, who provided us assistance with the microprobe. Gabriel Orozco, Valentina Astudillo, and Oliver Cooper are thanked for their assistance in the field and further discussion. CONAF authorized scientific research in this protected area and DIFROL provided logistical support during the 2013 field campaign.

Appendix A. Supplementary data

Supplementary data associated with this article (Tables S.1, S.2, S.3 and S.4) can be found in the online version, at doi: http://dx.doi.org/10.1016/j.jvolgeores.2017.05.035.

References

Anderson, D.L., 2000. The thermal state of the upper mantle; no role for mantle plumes. Geophys. Res. Lett. 27:3623–3626. http://dx.doi.org/10.1029/2000GL011533.
Anderson, D.L., 2001. Top-down tectonics? Science 293:2016–2018. http://dx.doi.org/10.1126/science.1065448.
Argus, D.F., Gordon, R.G., Heflin, M.B., Ma, C., Eanes, R.J., Willis, P., Peltier, W.R., Owen, S.E., 2010. The angular velocities of the plates and the velocity of Earth's centre from space geodesy. Geophys. J. Int. 180:913–960. http://dx.doi.org/10.1111/j.1365-246X.2009.04463.x.
Baker, P.E., Gledhill, A., Harvey, P.K., Hawkesworth, C.J., 1987. Geochemical evolution of the Juan Fernandez Islands, SE Pacific. J. Geol. Soc. Lond. 144:933–944. http://dx.doi.org/10.1144/gsjgs.144.6.0933.
Ballmer, M.D., van Hunen, J., Ito, G., Tackley, P.J., Bianco, T.a., 2007. Non-hotspot volcano chains originating from small-scale sublithospheric convection. Geophys. Res. Lett. 34. http://dx.doi.org/10.1029/2007GL031636.
Ballmer, M.D., Ito, G., van Hunen, J., Tackley, P.J., 2011. Spatial and temporal variability in Hawaiian hotspot volcanism induced by small-scale convection. Nat. Geosci. 4:457–460. http://dx.doi.org/10.1038/ngeo1187.
Beattie, P., 1993. Olivine-melt and orthopyroxene-melt equilibria. Contrib. Mineral. Petrol. 115:103–111. http://dx.doi.org/10.1007/BF00712982.
Bianco, T.A., Ito, G., Becker, J.M., Garcia, M.O., 2005. Secondary Hawaiian volcanism formed by flexural arch decompression. Geochem. Geophys. Geosyst. 6:1–24. http://dx.doi.org/10.1029/2005GC000945.
Bonatti, E., 1990. Not so hot "hot spots" in the oceanic mantle. Science 250:107–111. http://dx.doi.org/10.1126/science.250.4977.107.
Booker, J., Bullard, E.C., Grasty, R.L., 1967. Palaeomagnetism and age of rocks from Easter Island and Juan Fernandez. Geophys. J. Int. 12:469–471. http://dx.doi.org/10.1111/j.1365-246X.1967.tb03127.x.
Boudier, F., 1991. Olivine xenocrysts in picritic magmas - an experimental and microstructural study. Contrib. Mineral. Petrol. 109:114–123. http://dx.doi.org/10.1007/BF00687204.
Chatterjee, N., Bhattacharji, S., Fein, C., 2005. Depth of alkalic magma reservoirs below Kolekole cinder cone, Southwest rift zone, East Maui, Hawaii. J. Volcanol. Geotherm. Res. 145:1–22. http://dx.doi.org/10.1016/j.jvolgeores.2005.01.001.
Clague, D.A., 1987. Hawaiian xenolith populations, magma supply rates, and development of magma chambers. Bull. Volcanol. 49:577–587. http://dx.doi.org/10.1007/BF01079963.
Clouard, V., Bonneville, A., 2001. How many Pacific hotspots are fed by deep-mantle plumes? Geology 29 (8):695–698. http://dx.doi.org/10.1130/0091-7613(2001)029<0695:HMPHAF>2.0.CO;2.
Courtillot, V., Davaille, A., Besse, J., Stock, J., 2003. Three distinct types of hotspots I the Earth's mantle. Earth Planet. Sci. Lett. 205:295–308. http://dx.doi.org/10.1016/S0012-821X(02)01048-8.
Davidson, J.P., Morgan, D.J., Charlier, B.L.A., Harlou, R., Hora, J.M., 2007. Microsampling and isotopic analysis of igneous rocks: Implications for the study of magmatic systems. Annu. Rev. Earth Planet. Sci. 35:273–311. http://dx.doi.org/10.1146/annurev.earth.35.031306.140211.
Devey, C.W., Hemond, C., Stoffers, P., 2000. Metasomatic reactions between carbonated plume melts and mantle harzburgite: the evidence from Friday and Domingo Seamounts (Juan Fernandez chain, SE Pacific). Contrib. Mineral. Petrol. 139:68–84. http://dx.doi.org/10.1007/s004100050574.
Dixon, J.E., Leist, L., Langmuir, C., Schilling, J.-G., 2002. Recycled dehydrated lithosphere observed in plume-influenced mid-ocean-ridge basalt. Nature 420:385–389. http://dx.doi.org/10.1038/nature01215.
Farley, K.A., Basu, A.R., Craig, H., 1993. He, Sr and Nd isotopic variations in lavas from the Juan Fernandez Archipelago, SE Pacific. Contrib. Mineral. Petrol. 115:75–87. http://dx.doi.org/10.1007/BF00712980.
Fisk, M.R., Upton, B.G.J., Ford, C.E., White, W.M., 1988. Geochemical and experimental study of the genesis of magmas of Reunion Island, Indian Ocean. J. Geophys. Res. Solid Earth 93:4933–4950. http://dx.doi.org/10.1029/JB093iB05p04933.
Fleck, R.J., Sutter, J.F., Elliot, D.H., 1977. Interpretation of discordant 40Ar/39Ar age-spectra of mesozoic tholeiites from antarctica. Geochim. Cosmochim. Acta 41:15–32. http://dx.doi.org/10.1016/0016-7037(77)90184-3.
Frey, F.A., Wise, W.S., Garcia, M.O., West, H., Kwon, S.-T., Kennedy, A., 1990. Evolution of Mauna Kea volcano, Hawaii: petrologic and geochemical constraints on postshield volcanism. J. Geophys. Res. 95:1271–1300. http://dx.doi.org/10.1029/JB095iB02p01271.
Garcia, M.O., 1996. Petrography and olivine and glass chemistry of lavas from the Hawaii scientific drilling project. J. Geophys. Res. Solid Earth 101:11701–11713. http://dx.doi.org/10.1029/95JB03846.
Garcia, M.O., Swinnard, L., Weis, D., Greene, A.R., Tagami, T., Sano, H., Gandy, C.E., 2010. Petrology, geochemistry and geochronology of Kaua'i lavas over 4–5 Myr: Implications for the origin of rejuvenated volcanism and the evolution of the Hawaiian plume. J. Petrol. 51:1507–1540. http://dx.doi.org/10.1093/petrology/egq027.
Garcia, M.O., Smith, J.R., Tree, J.P., Weis, D., Harrison, L., Jicha, B.R., 2015. Petrology, geochemistry, and ages of lavas from Northwest Hawaiian Ridge volcanoes. Geol. Soc. Am. Spec. Pap. 511. http://dx.doi.org/10.1130/2015.2511(01).
Geldmacher, J., Hoernle, K., 2000. The 72 Ma geochemical evolution of the Madeira hotspot (eastern North Atlantic): recycling of Paleozoic (<500 Ma) oceanic lithosphere. Earth Planet. Sci. Lett. 183:73–92. http://dx.doi.org/10.1016/S0012-821X(00)00266-1.
Gerlach, D.C., Hart, S.R., Morales, V.W.J., Palacios, C., 1986. Mantle heterogeneity beneath the Nazca plate: San Felix and Juan Fernandez islands. Nature 322:165–169. http://dx.doi.org/10.1038/322165a0.
Gurriet, P., 1987. A thermal model for the origin of post-erosional alkalic lava, Hawaii. Earth Planet. Sci. Lett. 82:153–158. http://dx.doi.org/10.1016/0012-821X(87)90115-4.
Hammer, J., Jacob, S., Welsch, B., Hellebrand, E., Sinton, J., 2016. Clinopyroxene in postshield Haleakala ankaramite: 1. Efficacy of thermobarometry. Contrib. Mineral. Petrol. 171:1–23. http://dx.doi.org/10.1007/s00410-015-1212-x.
Hansteen, T.H., Klügel, A., Schmincke, H.-U., 1998. Multi-stage magma ascent beneath the Canary Islands: evidence from fluid inclusions. Contrib. Mineral. Petrol. 132:48–64. http://dx.doi.org/10.1007/s004100050404.
Helz, R.T., Thornber, C.R., 1987. Geothermometry of Kilauea Iki lava lake, Hawaii. Bull. Volcanol. 49:651–668. http://dx.doi.org/10.1007/BF01080357.
Herzberg, C., O'Hara, M.J., 2002. Plume-associated ultramafic magmas of Phanerozoic age. J. Petrol. 43:1857–1883. http://dx.doi.org/10.1093/petrology/43.10.1857.
Hieronymus, C.F., Bercovici, D., 2000. Non-hot spot formation of volcanic chains: controls of tectonic stresses on magma transport. Earth Planet. Sci. Lett. 181:539–554. http://dx.doi.org/10.1016/S0012-821X(00)00227-2.
Hirano, N., Yamamoto, J., Kagi, H., Ishii, T., 2004. Young, olivine xenocryst-bearing alkali-basalt from the oceanward slope of the Japan Trench. Contrib. Mineral. Petrol. 148:47–54. http://dx.doi.org/10.1007/s00410-004-0593-z.
Hoernle, K., Schmincke, H.U., 1993. The petrology of the tholeiites through melilite nephelinites on Gran Canaria, Canary Islands: crystal fractionation, accumulation, and depths of melting. J. Petrol. 34:573–597. http://dx.doi.org/10.1093/petrology/34.3.573.
Irvine, T.N., Baragar, R.A., 1971. A guide to the chemical classification of the common volcanic rocks. Can. J. Earth Sci. 8 (5):523–548. http://dx.doi.org/10.1139/e71-055.

Kamenetsky, V.S., Elburg, M., Arculus, R., Thomas, R., 2006. Magmatic origin of low-Ca olivine in subduction-related magmas: co-existence of contrasting magmas. Chem. Geol. 233:346–357. http://dx.doi.org/10.1016/j.chemgeo.2006.03.010.
Konter, J.G., Jackson, M.G., 2012. Large volumes of rejuvenated volcanism in Samoa: Evidence supporting a tectonic influence on late-stage volcanism. Geochem. Geophys. Geosyst. 13. http://dx.doi.org/10.1029/2011GC003974.
Konter, J.G., Staudigel, H., Blichert-Toft, J., Hanan, B.B., Polvé, M., Davies, G.R., Shimizu, N., Schiffman, P., 2009. Geochemical stages at Jasper seamount and the origin of intraplate volcanoes. Geochem. Geophys. Geosyst. 10. http://dx.doi.org/10.1029/2008GC002236.
Lara, L.E., Moreno, H., Naranjo, J.A., Matthews, S., Pérez de Arce, C., 2006. Magmatic evolution of the Puyehue–Cordón Caulle Volcanic Complex (40° S), Southern Andean Volcanic Zone: from shield to unusual rhyolitic fissure volcanism. J. Volcanol. Geotherm. Res. 157:343–366. http://dx.doi.org/10.1016/j.jvolgeores.2006.04.010.
Le Maitre, R.W., 2002. Igneous Rocks – a Classification and Glossary of Terms. Cambridge University Press, Cambridge (236 pp.). http://dx.doi.org/10.1017/CBO9780511535581.
Li, C., Thakurta, J., Ripley, E.M., 2012. Low-Ca contents and kink-banded textures are not unique to mantle olivine: evidence from the Duke Island Complex, Alaska. Mineral. Petrol. 104:147–153. http://dx.doi.org/10.1007/s00710-011-0188-0.
Macdonald, G.A., Abbott, A.T., Peterson, F.L., 1983. Volcanoes in the Sea: the Geology of Hawaii. University of Hawaii Press, Honolulu (544 pp.).
Morales, A.J., 1987. Geología de las islas Robinson Crusoe y Santa Clara, Archipiélago Juan Fernández, V Región, Chile. Universidad Católica del Norte (103 pp.).
Morgan, W.J., 1971. Convection plumes in the lower mantle. Nature 230:42–43. http://dx.doi.org/10.1038/230042a0.
Morgan, W.J., 1972a. Deep mantle convection plumes and plate motions. Am. Assoc. Pet. Geol. Bull. 56 (2):203–213. http://dx.doi.org/10.1306/819A3E50-16C5-11D7-8645000102C1865D.
Morgan, W.J., 1972b. Plate motions and deep mantle convection. Geol. Soc. Am. Mem. 132:7–22. http://dx.doi.org/10.1130/MEM132-p7.
Natland, J.H., 2003. Capture of helium and other volatiles during the growth of olivine phenocrysts in picritic basalts from the Juan Fernandez Islands. J. Petrol. 44: 421–456. http://dx.doi.org/10.1093/petrology/44.3.421.
Nichols, A.R.L., Carroll, M.R., Höskuldsson, Á., 2002. Is the Iceland hot spot also wet? Evidence from the water contents of undegassed submarine and subglacial pillow basalts. Earth Planet. Sci. Lett. 202:77–87. http://dx.doi.org/10.1016/S0012-821X(02)00758-6.
Nimis, P., 1999. Clinopyroxene geobarometry of magmatic rocks. Part 2. Structural geobarometers for basic to acid, tholeiitic and mildly alkaline magmatic systems. Contrib. Mineral. Petrol. 135:62–74. http://dx.doi.org/10.1007/s004100050498.
Nimis, P., 2014. ResearchGate web. May 30, 2014. Last access May 2017. www.researchgate.net/post/Is_there_a_recent_model_for_pressure_estimates_from_clinopyroxene2.
Nimis, P., Ulmer, P., 1998. Clinopyroxene geobarometry of magmatic rocks part 1: an expanded structural geobarometer for anhydrous and hydrous, basic and ultrabasic systems. Contrib. Mineral. Petrol. 133:122–135. http://dx.doi.org/10.1007/s004100050442.
Orozco, G., 2016. Evolución estructural y tectónica de la isla Robinson Crusoe, Dorsal de Juan Fernández. Universidad de Chile (94 pp.).
Ozawa, A., Tagami, T., Garcia, M.O., 2005. Unspiked K–Ar dating of the Honolulu rejuvenated and Ko'olau shield volcanism on O'ahu, Hawai'i. Earth Planet. Sci. Lett. 232: 1–11. http://dx.doi.org/10.1016/j.epsl.2005.01.021.
Papike, J.J., Cameron, K.L., Baldwin, K., 1974. Amphiboles and pyroxenes; characterization of other than quadrilateral components and estimates of ferric iron from microprobe data. Geol. Soc. Am. Abstr. Programs 6, 1053–1054.
Paul, D., White, W.M., Blichert-Toft, J., 2005. Geochemistry of Mauritius and the origin of rejuvenescent volcanism on oceanic island volcanoes. Geochem. Geophys. Geosyst. 6. http://dx.doi.org/10.1029/2004GC000883.
Peltier, A., Bachèlery, P., Staudacher, T., 2009. Magma transport and storage at Piton de La Fournaise (La Réunion) between 1972 and 2007: a review of geophysical and geochemical data. J. Volcanol. Geotherm. Res. 184:93–108. http://dx.doi.org/10.1016/j.jvolgeores.2008.12.008.
Pietruszka, A.J., Heaton, D.E., Marske, J.P., Garcia, M.O., 2015. Two magma bodies beneath the summit of Kilauea Volcano unveiled by isotopically distinct melt deliveries from the mantle. Earth Planet. Sci. Lett. 413:90–100. http://dx.doi.org/10.1016/j.epsl.2014.12.040.
Poland, M.P., Miklius, A., Montgomery-Brown, E.K., 2014. Magma supply, storage, and transport at shield-stage Hawaiian volcanoes: chapter 5 in characteristics of Hawaiian volcanoes (RPRT). Professional Paper Reston, VA. http://dx.doi.org/10.3133/pp18015.
Putirka, K.D., 2008a. Thermometers and barometers for volcanic systems. Rev. Mineral. Geochem. 69:61–120. http://dx.doi.org/10.2138/rmg.2008.69.3.
Putirka, K., 2008b. Excess temperatures at ocean islands: implications for mantle layering and convection. Geology 36:283–286. http://dx.doi.org/10.1130/G24615A.1.
Putirka, K.D., Mikaelian, H., Ryerson, F., Shaw, H., 2003. New clinopyroxene-liquid thermobarometers for mafic, evolved, and volatile-bearing lava compositions, with applications to lavas from Tibet and the Snake River Plain, Idaho. Am. Mineral. 88: 1542–1554. http://dx.doi.org/10.2138/am-2003-1017.
Quensel, P., 1920. Additional comments on the geology of the Juan Fernandez Islands. In: Skottsberg, C. (Ed.), The Natural History of Juan Fernandez and Easter Island. Geography, Geology, Origin of Island Life vol. 1, pp. 37–88.
Renne, P.R., Deino, A.L., Walter, R.C., Turrin, B.D., Swisher, C.C., Becker, T.A., Curtis, G.H., Sharp, W.D., Jaouni, A.-R., 1994. Intercalibration of astronomical and radioisotopic time. Geology 22:783–786. http://dx.doi.org/10.1130/0091-7613(1994)022<0783:IOAART>2.3.CO;2.
Ribe, N.M., Christensen, U.R., 1999. The dynamical origin of Hawaiian volcanism. Earth Planet. Sci. Lett. 171:517–531. http://dx.doi.org/10.1016/S0012-821X(99)00179-X.
Rodrigo, C., Lara, L., 2014. Plate tectonics and the origin of the Juan Fernández Ridge: analysis of bathymetry and magnetic patterns. Lat. Am. J. Aquat. Res. 42 (4):907–917. http://dx.doi.org/10.3856/vol42-issue4-fulltext-15.
Roeder, P.L., Emslie, R.F., 1970. Olivine-liquid equilibrium. Contrib. Mineral. Petrol. 29: 275–289. http://dx.doi.org/10.1007/BF00371276.
Rohrbach, A., Schuth, S., Ballhaus, C., Münker, C., Matveev, S., Qopoto, C., 2005. Petrological constraints on the origin of arc picrites, New Georgia Group, Solomon Islands. Contrib. Mineral. Petrol. 149:685–698. http://dx.doi.org/10.1007/s00410-005-0675-6.
Ruprecth, P., Plank, T., 2013. Feeding andesitic eruptions with a high-speed connection from the mantle. Nature 500:68–72. http://dx.doi.org/10.1038/nature12342.
Ryan, M.P., 1988. The mechanics and three-dimensional internal structure of active magmatic systems: Kilaue volcano, Hawaii. J. Geophys. Res. 93:4213–4248. http://dx.doi.org/10.1029/JB093iB05p04213.
Simkin, T.O.M., Smith, J.V., 1970. Minor-element distribution in olivine. J. Geol. 78: 304–325. http://dx.doi.org/10.1086/627519.
Sobolev, A.V., Hofmann, A.W., Sobolev, S.V., Nikogosian, I.K., 2005. An olivine-free mantle source of Hawaiian shield basalts. Nature 434:590–597. http://dx.doi.org/10.1038/nature03411.
Sobolev, A.V., Hofmann, A.W., Kuzmin, D.V., Yaxley, G.M., Arndt, N.T., Chung, S.-L., Danyushevsky, L.V., Elliott, T., Frey, F.A., Garcia, M.O., Gurenko, A.A., Kamenetsky, V.S., Kerr, A.C., Krivolutskaya, N.A., Matvienkov, V.V., Nikogosian, I.K., Rocholl, A., Sigurdsson, I.A., Sushchevskaya, N.M., Teklay, M., 2007. The amount of recycled crust in sources of mantle-derived melts. Science 316:412–417. http://dx.doi.org/10.1126/science. 1138113.
Steinberger, B., O'Connell, R.J., 1998. Advection of plumes in mantle flow: implications for hotspot motion, mantle viscosity and plume distribution. Geophys. J. Int. 132: 412–434. http://dx.doi.org/10.1046/j.1365-246x.1998.00447.x.
Straub, S.M., Gomez-Tuena, A., Stuart, F.M., Zellmer, G.F., Espinasa-Perena, R., Cai, Y., Iizuka, Y., 2011. Formation of hybrid arc andesites beneath thick continental crust. Earth Planet. Sci. Lett. 303:337–347. http://dx.doi.org/10.1016/j.epsl.2011.01.013.
Stuessy, T.F., Foland, K.A., Sutter, J.F., Sanders, R.W., Silva, M., 1984. Botanical and geological significance of potassium-argon dates from the Juan Fernandez Islands. Science 225 (80):49–51. http://dx.doi.org/10.1126/science.225.4657.49.
Tilling, R.I., Kauahikaua, J.P., Brantley, S.R., Neal, C.A., 2014. The Hawaiian volcano observatory: a natural laboratory for studying basaltic volcanism: chapter 1 in characteristics of Hawaiian volcanoes (RPRT). Professional Paper Reston, VA. http://dx.doi.org/10.3133/pp18011.
Vergara, H., Morales, E., 1985. Morofología submarina del segmento central del cordón asísimico Juan Fernández. In: Arana, P. (Ed.), Investigaciones marinas en el archipiélago de Juan Fernández. Universidad Católica de Valparaíso, Valparaíso, pp. 25–34.
Von Huene, R., Corvalán, J., Flueh, E.R., Hinz, K., Korstgard, J., Ranero, C.R., Weinrebe, W., 1997. Tectonic control of the subducting Juan Fernández Ridge on the Andean margin near Valparaiso, Chile. Tectonics 16:474–488. http://dx.doi.org/10.1029/96TC03703.
Wang, Z., Gaetani, G.A., 2008. Partitioning of Ni between olivine and siliceous eclogite partial melt: experimental constraints on the mantle source of Hawaiian basalts. Contrib. Mineral. Petrol. 156:661–678. http://dx.doi.org/10.1007/s00410-008-0308-y.
Weis, D., Frey, F.A., Giret, A., Cantagrel, J.M., 1998. Geochemical characteristics of the youngest volcano (Mount Ross) in the Kerguelen Archipelago: inferences for magma flux, lithosphere assimilation and composition of the Kerguelen plume. J. Petrol. 39:973–994. http://dx.doi.org/10.1093/petroj/39.5.973.
Welsch, B., Hammer, J., Baronnet, A., Jacob, S., Hellebrand, E., Sinton, J., 2016. Clinopyroxene in postshield Haleakala ankaramite: 2. Texture, compositional zoning and supersaturation in the magma. Contrib. Mineral. Petrol. 171:1–19. http://dx.doi.org/10.1007/s00410-015-1213-9.
White, W.M., Duncan, R.A., 1996. Geochemistry and geochronology of the Society Islands: new evidence for deep mantle recycling. Earth Processes: Reading the Isotopic Code. American Geophysical Union:pp. 183–206 http://dx.doi.org/10.1029/GM095p0183.
Woodhead, J.D., 1992. Temporal geochemical evolution in oceanic intra-plate volcanics: a case study from the Marquesas (French Polynesia) and comparison with other hotspots. Contrib. Mineral. Petrol. 111:458–467. http://dx.doi.org/10.1007/BF00320901.
Wright, E., White, W.M., 1987. The origin of Samoa: new evidence from Sr, Nd, and Pb isotopes. Earth Planet. Sci. Lett. 81:151–162. http://dx.doi.org/10.1016/0012-821X(87)90152-X.